SUPPLEMENTAL DATA

SUPPLEMENTAL METHODS

Patient materials

We collected in this retrospective study lymphoma samples of the collaborating centers from 15 patients diagnosed with Burkitt lymphoma (BL), atypical BL/BL-like or high grade B-cell lymphoma (range 4-52 years at diagnosis) including three previously published cases [1–3] (refer to the attached photomicrographs of the HE stained sections of the cases in Supplemental Appendix 1). Of note is, that due to the way the cases were selected they are not population-based, and hence, we cannot exclude a recruitment bias. During routine diagnostics, those cases were shown to be IG-*MYC* negative by molecular cytogenetics applying different FISH probes including *MYC* break apart, IGH-, IGL- or IGK-*MYC* fusion probes (refer to the supplemental chapter fluorescence in situ hybridization). Based on tumor cell morphology and growth pattern, the cases were retrospectively analyzed for the occurrence of the peculiar 11q aberration by fluorescence in situ hybridization. This pattern was either the typical 11q-gain/loss or solely an 11q25-qter loss in agreement with the published case by Salaverria *et* al. [2]. The presence of the 11q aberration was verified using SNP-array profiling. Accordingly, the 11q aberration pattern of the cases studied herein differs from that observed in some DLBCL, which carry a gain in 11q24.3 instead of a loss (or loss of heterozygosity) as found in the cases analyzed herein [4,5]. The lack of an IG-*MYC* translocation and presence of 11q aberration together with the morphological and immunophenotypical findings, led to the retrospective classification as *MYC*-negative Burkitt-like lymphoma with 11q aberration (mnBLL,11q,).

The immunophenotypic characterization by immunohistochemistry of the cases was performed by the individual centers submitting the cases. Supplemental Table 1 shows an overview of the clinical, cytogenetic and immunophenotypic characteristics of the mnBLL,11q, cases studied herein.

This study was approved by local review boards and performed in line with the regulations of the Institutional Review Board of the Medical Faculty of the University Kiel (D425/03, and D447/10 and amendment from 09.03.2010).

Fluorescence in situ hybridization

If not obtained from previous publications or the original data from the individual centers submitting cases, FISH analyses were performed as described in the following. Extraction and labeling of BAC DNA for homemade assays, preparation of slides and hybridization on formalin fixed paraffin embedded (FFPE) tissue sections were performed as previously described [6].

The locus-specific probes LSI BCL6, LSI MYC, LSI IGH/MYC and LSI BCL2 were applied (Abbott Molecular Diagnostics,Wiesbaden-Delkenheim, Germany). For the detection of IGK-*MYC* and IGL-*MYC* translocations non-commercial probes were applied [7,8]. Additionally, we applied a non-commercial assay to detect the peculiar pattern of chromosomal gain and loss on 11q modified from Salaverria et al. [2]. This assay contained the clones RP11-629A20 (11q24.3) labelled in spectrum orange, RP11-414G21 (11q23.3) labelled in spectrum green and a commercially available chromosome 11 enumeration probe labelled in spectrum aqua as control (CEP11, D11Z1 from Abbott, Wiesbaden, Germany). Evaluation of slides was performed using a Zeiss fluorescence microscope equipped with appropriate filter sets. Whenever possible for all FISH analyses at least 100 nuclei were analysed for each probe. Acquisition and processing of digital images were performed using the ISIS FISH Imaging System V5.8 (MetaSystems, Altlussheim, Germany).

DNA extraction

Extraction of DNA from formalin-fixed paraffin-embedded (FFPE) tissue was performed using either the truXTRAC FFPE DNA micro Tube Kit (Covaris) or the Qiagen FFPE DNA extraction kit (Qiagen) according to manufacturers' protocols. The quality of the DNA was tested using the High Sensitivity DNA Assay on the 2100 Bioanalyzer (Agilent) to show a main peak above 200bp size. The quantity of the DNA was measured using Qubit fluorometer together with the Quant-iT dsDNA BR Assay Kit (Life Technologies).

OncoScan™ CNV FFPE Assay

Copy number analysis was performed on 12 mnBLL,11q, cases using the OncoScan™ CNV FFPE Assay Kit as described[9]. Data were mined for copy number alterations (regions of gain, loss and copy number neutral loss of heterozygosity) using OncoScan Console 1.3 (Affymetrix) and Nexus Express for OncoScan 3 (Biodiscovery). Alterations were mapped on human reference genome build GRCh37/hg19. Only chromosomal imbalances encompassing at least 20 informative probes and being larger than 100 kb as well as CNN-LOH larger than 5 Mb were considered informative.

Whole exome sequencing and data processing

Sequencing

Exome sequencing of 15 mnBLL,11q samples was performed as recently described[9] using the Agilent SureSelect v6 exome target enrichment kit. The library was sequenced on an Illumina HiSeq 4000 sequencing instrument (Illumina) using a paired-end 2 × 75 bp protocol.

Alignment and variant calling

Alignment and variant calling have been performed as recently described[9]. In short, sequencing reads were mapped to human reference genome (build 37, version hs37d5) (ftp://ftp.1000genomes.ebi.ac.uk/vol1/ftp/technical/reference/phase2_reference_assembly_sequence/hs37d5.fa.gz) with bwa-mem (version 0.7.8, minimum base quality threshold set to zero [-T 0], remaining settings left to default)[10]. Coordinates were sorted with bamsort (compression option set to fast[11] and duplicate read pairs were marked with bammarkduplicates (compression option set to best, both are part of the biobambam package (version 0.0148).

Single nucleotide variants (SNVs) and indels were called from tumor samples with the internal DKFZ pipeline based on samtools/bcftools 0.1.19 and custom filters (optimized for somatic variant calling by deactivating the pval-threshod in bcftools) and Platypus 0.8.1, respectively as described by Jabs *et* al.[12]. Genes were annotated with Annovar (Feb 2016). A 'confidence score' was calculated for each mutation. The maximum allowed allele frequency in ExAC[13] was lowered to 0.0001% (non-TCGA variants). Furthermore, variants with possibly base quality bias or a mapping quality bias (corresponding PV4 p-value < 0.01) were excluded from analysis. More cohort-based filtering criteria were applied downstream of the individual variant calling. In order to remove recurrent artifacts and misclassified germline events, somatic indels, that were identified as germline in at least two patients of the ICGC MMML-Seq whole-genome sequencing (WGS) cohort which encompasses more than 250 paired tumor-and non-tumor samples were excluded.

Finally, variants in artifact prone regions were removed. These artifact prone regions were identified in an in-house lymphoma exome cohort consisting of more than 100 whole-exome sequencing (WES) data sets from diverse lymphoma FFPE samples, which all have been applied to the same sequencing pipeline. Variants in regions with between two and four variants with maximum intermutation distance of 100 bp that were recurrently found in three or more patients were considered artifacts, unless these regions overlapped with recurrent Kataegis regions[14] defined by the above described in-house whole genome sequencing lymphoma cohort. Of note, despite thorough filtering, most likely some germline variants remained in the final data set. We cross-referenced the list of recurrently mutated genes in mnBLL,11q, with genes published by Lawrence *et* al.[15] that can be considered as large and/or late replicating genes likely constituting artifacts or passenger mutations. This refers to three genes frequently mutated in mnBLL,11q, including *TTN*, *MUC16* and *MUC5B*.

GNA13 and *NFRKB* mutation verification by Sanger sequencing

To verify the mutations in *GNA13* and *NFRKB* identified by WES primers were designed to cover the mutations. PCR primers and PCR conditions for Sanger sequencing of are listed in Supplemental Table 4. After PCR, products were subjected to Sanger sequencing using the Big Dye Terminator v1.1 Cycle Sequencing Kit (Life Technologies). Sequence analysis was performed using an ABI PRISM 3130 Genetic Analyzer.

Mutation modeling

Predictions of the effects of non-synonymous coding mutations have been carried out using Mutation Assessor [16], VEP [17] and Mechismo [18]. Mutation annotations on protein primary sequence has been done through the Lollipops software [19]. Post translational modification information has been obtained from PhosphositePlus [20].

The model of full length GNA13 alpha subunit has been obtained through Modeller [21] by using as multiple templates the structures of GNA13 (PDB ID: 3AB3) and GNAS (PDB ID: 3SN6). The prototypical structure of ADRB2 receptor complexed to Gs heterotrimer (PDB ID: 3SN6) has been used as a template to model the complex, by replacing the model of GNA13 with the structure of GNAS.

SUPPLEMENTAL RESULTS AND DISCUSSION

Statistics of whole exome sequencing

Analyzing the mutational profile (single nucleotide variants and small insertions/deletions) of the mnBLL,11q, using WES, we identified a median of 528 (260-1224) variants including a median of 200 (range 121-522) potentially protein-changing alterations. Despite excessive filtering and based on extensive controls of the pipeline we have to take into account that the given numbers include a series of false positive calls i.e. misclassified germline variants.

TTN mutations

To accumulate further evidence that the *TTN* mutations constitute likely passenger mutations, we interrogated the mutation frequency of *TTN* in the projects of ICGC (https://dcc.icgc.org/) as well as TCGA (https://portal.gdc.cancer.gov/) in which in the majority tumor and matched normal control from the same donor has been sequenced. In 61/72 ICGC projects and 26/33 TCGA projects *TTN* mutations occur in more than 10% of cases which further supports that these mutations should be rather considered as passenger mutations.

Functional consequence of NFRKB mutations

We observed *NFRKB* mutations in four of the mnBLL,11q, cases. By definition of the disease, the loss in 11q24 leads to the deletion of the second *NFRKB* allele. Thus, the tumor cells of these cases carried only the mutated allele. We observed three stopgain mutations, R290*, K322* and Q1103*, as well as a missense R174C mutation. The latter is predicted to perturb adjacent phosphosites (see Figure 2). Most likely, the stopgain mutations lead to nonsense-mediated decay (NMD) and, thus, to complete loss of functional *NFRKB* protein expression. We nevertheless explored whether there could be some residual function of the truncated proteins. The INO80 subunit NFRKB is a DNA-binding transcriptional activator. In line with this and the function of the INO80 complex in nucleosome remodeling, NFRKB exerts its function in the nucleus. Here, NFRKB forms a complex with the deubiquitinating enzyme UCHL5 (Uch37) and other members of the INO80 complex [22,23]. As a prerequisite, transport of the NFRKB protein has to be assured. ELM predicts nuclear localization signals (NLS) between amino acids 295 and 325 of NFRKB. Thus, R290* deletes the predicted NLS and the K322* likely disrupts the NLS. Though we cannot exclude other, not predicted NLS or alternative shuttling mechanisms to the nucleus, these findings suggest again complete ablation of NFRKB nuclear function. Despite this strong evidence against a remnant nuclear function of NFRKB, we explored published *in vitro* data to investigate the potential impact of the detected *NFRKB* (INO80G) mutations on the INO80 complex. Sahtoe et al.[24] tested different truncated forms of NFRKB with regard to UCHL5 activation. They showed, that truncated forms of NFRKB, comprising the entire N-terminal DEU domain (amino acids 39-170), lead to inhibition

of UCHL5. Based on these *in vitro* results, the most obvious interpretation of the stopgain mutants (R290* and K322*) in the two mnBLL,11q, cases would be that they lead to a NFRKB-DEU fragment that persistently inhibits UCHL5. As a consequence, UCHL5 would not deubiquitinate its substrates leading to impairment of UCHL5 mediated activation of the complex [23]. Finally, the two stop gain mutations R290* and K322* are predicted to delete the protein region responsible for mediating interactions with transcriptional regulators and/or DNA. In summary, whatever of the four mechanisms (NMD, loss of nuclear localization, inactivation of UCHL5 or loss of DNA binding) is the most prominent in the tumor cells, at least the two stop gain mutations R290* and K322* mutations are predicted to abolish the NFRKB function. The R174C mutation is predicted to perturb adjacent phosphosites, e.g. S176 and is located in a motif predicted by ELM (elm.eu.org) to be either a phosphorylation site of GSK3 and MAP kinase or a docking site for USP7 or the Pin1 WW domain. The C-terminal deletion by Q1103* is predicted to have detrimental consequences, as it is rich in phosphorylation sites (e.g. CK1 and GSK3) or recognition sites for FHA and WDR5.

In consequence, there is considerable evidence from *in vitro* and structural biology data that the mutations in *NFRKB* wipe out its function. As NFRKB is a DNA-binding protein we next explored ChIP-Seq data from the ENCODE project [25] for NFRKB (in K562 cells) available through the CISTROME data browser (http://www.cistrome.org/, accessed 30.10.2018). Remarkably, we detected ChIP-Seq peaks of NFRKB around the transcription start sites of all five differentially overexpressed genes in the 11q minimal region of gain between cases with 11q-gain/loss pattern and IG-*MYC* BL (*IL10RA, ZNF259, PAFAH1B2, CEP164, SIDT2*) but not any of the genes in the minimal region of (homozygous) loss in 11q24 (*ETS1, FLI1, KCNJ1, KCNJ5, C11Orf45, TP53AIP1, ARHGAP32*) [2]. Thus, it is intriguing to speculate that the predicted loss of NFRKB binding and function in the minimal region of gain might be associated with the amplification of the region through altered nucleosome modelling and/or increase gene expression due to altered transcriptional control.

SUPPLEMENTAL TABLES

Supplemental Table 1

Overview of molecular cytogenetic and immunophenotype profile of mnBLL,11q, cases.

Case	Clinical data				Molecular Cytogenetics (FISH)				CN profile	Immunophenotype						Growth pattern		Immune status
	Morphological diagnosis	Age (yrs)	Sex	Site	11q gain/loss	MYC status	BCL2 status	BCL6 status	11q gain/loss	CD20	CD10	BCL2	BCL6	EBV	Ki-67	starry sky	other	
4130889[a]	BL[c]	22	M	Inguinal LN	n.a.	neg	neg	neg	pos	+	+	-	-	-	>95%	+	-	n.a.
4132029[a]	BL[c]	37	F	Cervical LN	n.a.	neg	neg	neg	pos	+	+	-	+	-	>95%	+	-	n.a.
4128648[b]	atypical BL[d]	9	M	Inguinal LN	n.a.	neg	n.a.	n.a.	pos	+	+	-	+	-	100	+	-	n.a.
4129295	BL[e]	4	M	Cervical LN	pos	neg	neg	neg	pos	+	+	-/+	n.a.	-	>95%	+	-	c
4126556	FL Grade 3B +DLBCL[e]	17	M	Cervical LN	pos	neg	neg	neg	pos	+	+	-	+	-	95%	-	+ (F)	c
4140575	aggressive mature B-cell lymphoma[e]	10	M	Iliac crest	pos	neg	neg	neg	pos	+	+	-	n.a.	-	100%	-	+ (D)	ID
4131149	atypical BL/ BL-like[e]	13	F	Appendix	pos	neg	neg	neg	pos	+	+	-	n.a.	-	~90%	+	-	c
4126517	DLBCL[e]	52	M	Appendix	pos	neg	neg	neg	pos	+	+	-	n.a.	-	>90%	-	+ (N)	PT
4132817	BL[e]	14	F	Abdominal tumor	pos	neg	neg	neg	pos	+	+	-	n.a.	-	90%	+	-	c
4144899	Aggressive B-cell lymphoma with follicular pattern[d]	14	M	Cervical LN	pos	neg	neg	neg	pos	+	+	-	+	-	>95%	+	+ (F)	n.a.
4146703	atypical BL/ BL-like[f]	21	M	Ileum/Colon	pos	neg	neg	neg	pos	+	+	-	+	-	~100%	+	-	n.a.
4179429	B-cell lymphoma[e]	22	M	Abdominal tumor	pos	neg	neg	neg	pos	+	+	-	+	-	~100%	+	-	c
4180189	BL[e]	7	M	Ileum	pos	neg	n.a.	n.a.	pos	+	+	+	+	-	~100%	+	-	c
4180310	atypical BL/ BL-like[f]	51	F	LN	pos*	neg	neg	neg	pos*	+	-	+/-	+/-	-	>90%	+	-	n.a.
4181370	high grade B-cell lymphoma[g]	21	M	Cervical LN	pos*	neg	neg	neg	pos*	+	+	-	+	-	>95%	+	+ (D)	c

[a] cases have been already published in [1–3]; [b] case has been published in [2]

[c] diagnosis reported by G.R., [d] diagnosis reported by ES.J., [e] diagnosis reported by W.K., [f] diagnosis reported by G.O., [g] diagnosis reported by L.L.,

Age (yrs): age at diagnosis in years; M: Male; F: Female; Site: localization of the tumor analyzed in this study; LN: lymph node; n.a.: not available, neg/-: negative; pos/+: positive; EBV: EBV status determined using EBER ISH; (F): follicular growth pattern; (D): diffuse growth pattern; (N): necrotic tissue; Immune status: PT: post-transplant; ID: immune defect; c: immune competent. * indicates that only a deletion of chromosome 11q was detected by FISH and OncoScan analysis (Supplemental Figure 1).

Supplemental Table 2

Overview of copy number alterations in the 12 mnBLL,11q, cases not yet published as identified by OncoScan analysis.

Case	Event	Chromosomal region in bp (hg19)	Cytoband	Length in bp
4129295	CN Gain	chr11:192,764-127,778,007	11p15.5 - q24.2	127585244
	CN Loss	chr11:127,799,447-133,280,976	11q24.2 - q25	5481530
	CN Gain	chr11:133,305,660-134,938,847	11q25	1633188
	CN Loss	chr14:86,454,666-88,383,985	114q31.3	1929320
	CN Loss	chrY:2,660,163-28,799,935	Yp11.31 - q11.23	26139773
4126556	CN Loss	chr1:5,126,273-7,758,760	1p36.32 - p36.23	2632488
	CN Gain	chr8:104,078,514-146,292,734	8q22.3 - q24.3	42214221
	CN Gain	chr11:58,169,996-122,984,689	11q12.1 - q24.1	64814694
	CN Loss	chr11:122,996,050-134,938,847	11q24.1 - q25	11942798
	CN Gain	chr12:1-133,851,895	12p13.33 - q24.33	133851895
4140575	CN Gain	chr11:1-119,724,987	11p15.5 - q23.3	119724987
	CN Loss	chr11:119,742,279-134,938,847	11q23.3 - q25	15196569
	CN Gain	chr12:1-133,851,895	12p13.33 - q24.33	133851895
4131149	High Copy Gain	chr1:157,503,805-157,840,353	1q23.1	336549
	CNN-LOH	chr2:21,494-52,395,370	2p25.3 - p16.3	52373877
	CN Gain	chr2:52,609,707-58,441,542	2p16.3 - p16.1	5831836
	High Copy Gain	chr2:58,465,027-64,441,643	2p16.1 - p14	5976617
	CN Loss	chr2:64,464,389-67,796,331	2p14	3331943
	High Copy Gain	chr2:67,875,117-68,354,727	2p14	479611
	CN Gain	chr3:187,435,688-188,540,034	3q27.3 - q28	1104347
	CN Loss	chr6:74,785,926-128,946,424	6q13 - q22.33	54160499
	CN Gain	chr7:41,421-62,008,916	7p22.3 - q11.21	61967496
	CN Loss	chr7:62,030,337-87,179,086	7q11.21 - q21.12	25148750
	CN Loss	chr7:105,310,593-105,679,551	7q22.3	368959
	CNN-LOH	chr7:103,595,652-159,118,443	7q22.1 - q36.3	55522792
	CN Gain	chr7:105,691,096-159,118,443	7q22.3 - q36.3	53427348
	CN Loss	chr9:35,291,473-36,343,643	9p13.3 - p13.2	1052171
	CN Loss	chr9:37,814,873-44,893,094	9p13.2 - p11.2	7078222
	CN Gain	chr9:123,778,148-124,132,880	9q33.2	354733
	CN Gain	chr11:58,312,880-87,197,069	11q12.1 - q14.2	28884190
	CN Loss	chr11:87,220,603-88,256,603	11q14.2	1036001
	CN Gain	chr11:103,206,043-120,931,054	11q22.3 - q23.3	17725012
	CN Loss	chr11:120,941,583-128,081,710	11q23.3 - q24.3	7140128
	CNN-LOH	chr11:128,081,710-128,617,231	11q24.3	535522
	CN Loss	chr11:128,617,231-134,938,847	11q24.3 - q25	6321617
	High Copy Gain	chr12:11,866,063-11,990,610	12p13.2	124548
	CN Gain	chr13:41,076,410-41,665,956	13q14.11	589547
	CN Loss	chr13:82,992,756-84,280,698	13q31.1	1287943
	CN Gain	chr13:84,302,618-86,213,498	13q31.1	1910881
	High Copy Gain	chr13:86,230,143-97,991,179	13q31.1 - q32.1	11761037
	CN Loss	chr13:98,000,888-99,676,650	13q32.1 - q32.3	1675763

	High Copy Gain	chr13:99,685,378-101,287,404	13q32.3	1602027
	CN Loss	chr13:101,298,448-115,103,150	13q32.3 - q34	13804703
	High Copy Gain	chr14:96,031,957-96,178,323	14q32.13	146367
	CN Loss	chr16:59,689,244-61,220,951	16q21	1531708
	CN Gain	chr16:63,963,839-64,975,148	16q21	1011310
	CN Loss	chr16:68,038,763-69,115,649	16q22.1	1076887
	CN Loss	chr17:400,959-22,217,883	17p13.3 - p11.1	21816925
	CN Gain	chr17:77,846,012-78,858,662	17q25.3	1012651
	CN Loss	chr18:21,884,848-28,183,403	18q11.2 - q12.1	6298556
	CN Gain	chr20:46,043,982-46,286,406	20q13.12	242425
4126517	CN Loss	chr3:48,179,178-54,819,686	3p21.31 - p14.3	6640509
	CNN-LOH	chr4:71,566-15,826,558	4p16.3 - p15.32	15754993
	CN Loss	chr10:73,667,572-94,571,124	10q22.1 - q23.33	20903553
	High Copy Gain	chr11:86,160,140-104,194,241	11q14.2 - q22.3	18034102
	CN Gain	chr11:104,214,465-116,826,870	11q22.3 - q23.3	12612406
	High Copy Gain	chr11:116,829,200-119,488,812	11q23.3	2659613
	CN Loss	chr11:119,502,703-134,938,847	11q23.3 - q25	15436145
	High Copy Gain	chr13:40,604,915-47,851,782	13q14.11 - q14.2	7246868
	CN Gain	chr13:58,232,774-90,952,373	13q21.1 - q31.3	32719600
	High Copy Gain	chr13:90,969,866-94,073,164	13q31.3	3103299
	CN Loss	chr13:94,080,307-115,103,150	13q31.3 - q34	21022844
	CNN-LOH	chr17:400,959-20,539,358	17p13.3 - p11.2	20138400
4132817	CNN-LOH	chr1:754,192-61,792,008	1p36.33 - p31.3	61037817
	CNN-LOH	chr5:1-180,364,100	5p15.33 - q35.3	180364100
	CN Loss	chr5:180,365,103-180,698,312	5q35.3	333210
	CNN-LOH	chr9:93,708,178-102,619,453	9q22.2 - q31.1	8911276
	CN Loss	chr9:102,639,361-108,417,743	9q31.1 - q31.2	5778383
	High Copy Gain	chr11:60,452,977-64,789,194	11q12.2 - q13.1	4336218
	CN Gain	chr11:64,793,738-120,398,613	11q13.1 - q23.3	55604876
	CN Loss	chr11:120,408,071-127,397,904	11q23.3 - q24.2	6989834
	Homozygous Copy Loss	chr11:127,422,804-129,014,488	11q24.2 - q24.3	1591685
	CN Loss	chr11:129,037,606-134,938,847	11q24.3 - q25	5901242
4144899	CN Gain	chr7:1-159,138,663	7p22.3 - q36.3	159138663
	CN Gain	chr14:20,219,083-106,097,037	14q11.2 - q32.33	85877955
	CN Gain	chr15:20,161,372-77,660,345	15q11.1 - q24.3	57498974
	CN Gain	chrX:1-155,270,560	Xp22.33 - q28	155270560
	CN Gain	chr5:1-180,915,260	5p15.33 - q35.3	180915260
	CN Gain	chr21:9,648,315-48,097,610	21p11.2 - q22.3	38449296
	CN Gain	chr11:59,852,596-120,890,823	11q12.1 - q23.3	61038228
	CN Gain	chr12:189,400-133,818,115	12p13.33 - q24.33	133628716
	CN Loss	chr11:120,907,482-134,938,847	11q23.3 - q25	14031366
	CN Loss	chr2:120,063,684-121,041,347	2q14.2	977664
4146703	CNN-LOH	chr1:149,044,448-249,212,878	1q21.2 - q44	100168431
	CN Gain	chr3:172,056,208-197,852,564	3q26.31 - q29	25796357
	High Copy Gain	chr11:74,145,528-108,384,207	11q13.4 - q22.3	34238680

	High Copy Gain	chr11:108,397,460-118,827,925	11q22.3 - q23.3	10430466
	CN Loss	chr11:118,846,574-134,938,847	11q23.3 - q25	16092274
	CN Gain	chr14:66,758,536-67,015,348	14q23.3	256813
4179429	CN Loss	chr1:2,709,392-9,798,054	1p36.32 - p36.22	7088663
	CN Loss	chr1:240,742,905-242,203,260	1q43	1460356
	High Copy Gain	chr11:64,299,110-65,140,209	11q13.1	841100
	CN Gain	chr11:65,157,820-109,380,008	11q13.1 - q22.3	44222189
	High Copy Gain	chr11:109,404,755-118,486,067	11q22.3 - q23.3	9081313
	CN Loss	chr11:118,501,459-134,938,847	11q23.3 - q25	16437389
	Homozygous Copy Loss	chrX:147,606,808-148,029,676	Xq28	422869
4180189	CN Gain	chr3:63,411-24,684,637	3p26.3 - p24.2	24621227
	CN Gain	chr3:26,685,232-60,492,152	3p24.1 - p14.2	33806921
	CN Gain	chr9:30,886,614-32,018,100	9p21.1	1131487
	CN Gain	chr11:71,914,724-103,813,331	11q13.4 - q22.3	31898608
	CN Loss	chr11:103,836,859-114,077,813	11q22.3 - q23.2	10240955
	High Copy Gain	chr11:114,081,947-119,123,704	11q23.2 - q23.3	5041758
	CN Gain	chr11:119,125,745-120,702,378	11q23.3	1576634
	CN Loss	chr11:120,717,000-134,938,847	11q23.3 - q25	14221848
	CN Gain	chr12:47,770,834-126,782,566	12q13.11 - q24.32	79011733
	CNN-LOH	chr17:30,606,301-80,263,427	17q11.2 - q25.3	49657127
	CN Gain	chrX:122,647,089-123,553,985	Xq25	906897
4180310	CN Gain	chr5:171,129,907-180,698,312	5q35.1 - q35.3	9568406
	CNN-LOH	chr10:47,009,329-135,434,303	10q11.22 - q26.3	88424975
	CN Gain	chr11:69,449,533-69,480,191	11q13.3	30659
	CN Loss	chr11:121,665,295-134,938,847	11q24.1 - q25	13273553
	CN Gain	chr16:83,887-2,303,083	16p13.3	2219197
	CNN-LOH	chr19:247,232-13,221,838	19p13.3 - p13.2	12974607
4181370	CNN-LOH	chr1:144,009,053-249,212,878	1q21.1 - q44	105203826
	CN Gain	chr4:62,406,893-63,075,798	4q13.1	668906
	CNN-LOH	chr6:204,909-37,144,404	6p25.3 - p21.2	36939496
	CN Gain	chr11:110,879,863-112,008,978	11q23.1	1129116
	CN Loss	chr11:121,206,488-134,938,847	11q24.1 - q25	13732360
	CN Gain	chr12:1-133,851,895	12p13.33 - q24.33	133851895

CN: copy number, CNN-LOH: copy number neutral loss of heterozygosity

Supplemental Table 4

PCR primers and PCR conditions for Sanger sequencing applied for verification of *GNA13* and *NFRKB* mutations detected by whole-exome sequencing.

Gene	Case with mutation	Genomic region in bp (hg19)	Forward primer (5'-3') Reverse primer (5'-3')	Annealing Temp.[1]	PCR[2] (bp)
GNA13	4146703, 4126556	chr17:63010217-63010438	AAACCAAAGGCCGCAGAAAA TGTTTTCCGTGACGTGAAGG	60°C	224 bp
	4130889	chr17:63010356-63010564	ACAGCAAGTCTTTTGTACATCAC TCCCCACTGCTTAAGAGACG	60°C	209 bp
	4132029, 4132817	chr17:63010657-63010905	GACATTGCTGAAAACCCGGT CCCACCAAAGGCATCCATG	60°C	249 bp
	4132029, 4130889	chr17:63014306-63014554	ACATCGATATCCTGACTTCTGCT AGCTGTCTGAAATTGGTGACT	60°C	249 bp
	4132817	chr17:63049477-63049764	GCCTTAGCCTTTCAGTCTG GATGTCGTTTGATACCCGGG	55°C	288 bp
	4181370, 4128648	chr17:63052197-63052588	GGGAGACAAGCGGGAGAG AAGACCTATGTGAAGCGGCT	60°C	392 bp
NFRKB	4180189	chr11:129739500-129739695	CTTGGACACAGCAGCATTCA CACAGTGGCCTCTTCAGAAG	60°C	196 bp
	4144899	chr11:129752395-129752591	GTGCGACCCCTTCAGTACT TAAGACCCCTCACTTCCCTG	60°C	197 bp
	4146703	chr11:129752962-129753169	ACGCAACTTAACACCATAGTCA TGGCAAAGTCACCTCAGTTT	60°C	208 bp
	4126517	chr11:129755320-129755544	GGACACTCACCCTCTTCATCA CTTGGATGATGACTTGTACCCC	60°C	225 bp

[1] Annealing temperature in °C, [2] Length of PCR product in base pairs (bp)

SUPPLEMENTAL FIGURES

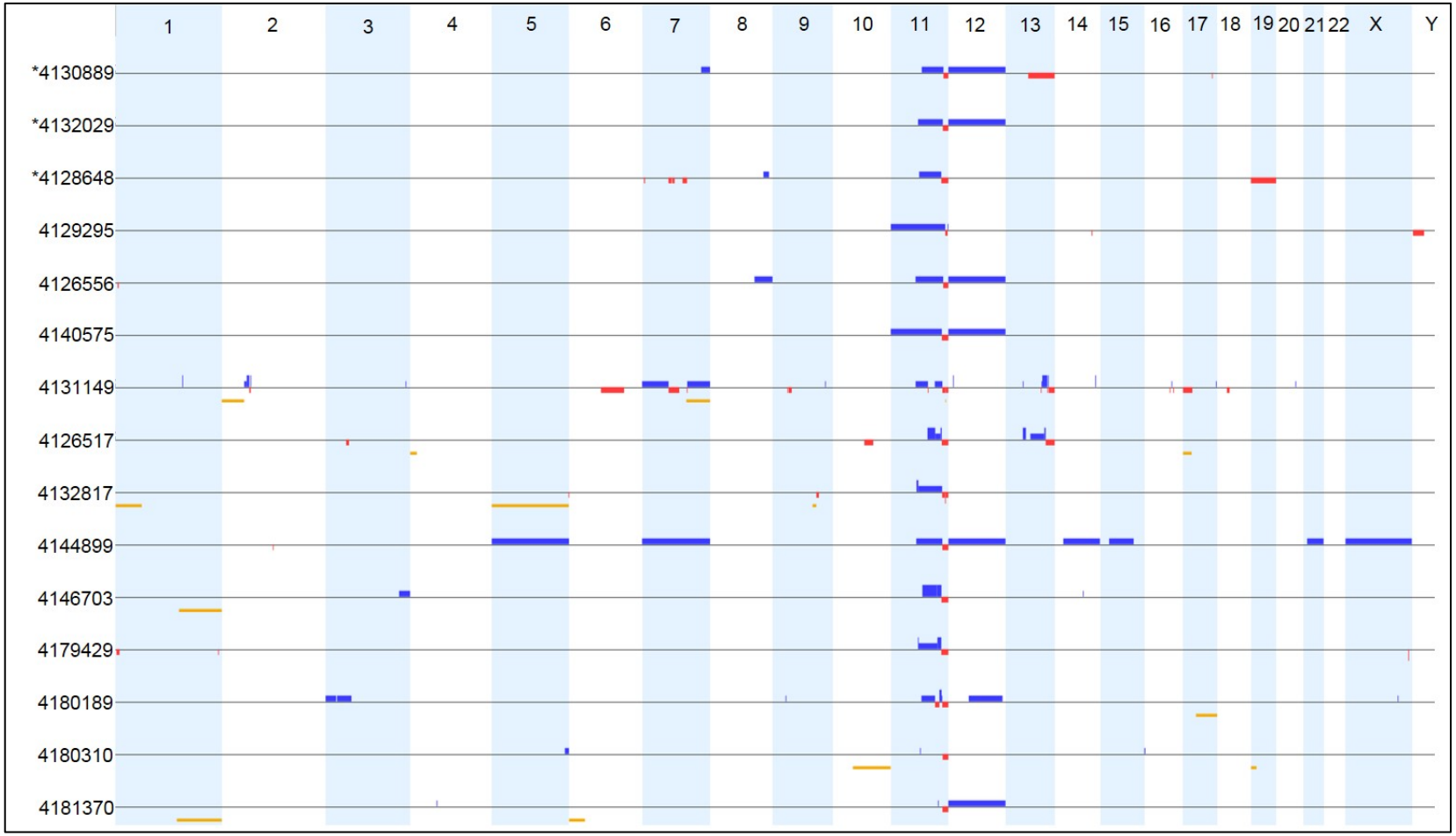

Supplemental Figure 1: Overview of the copy number alterations in 15 mnBLL,11q, cases (the asterisks indicate that these profiles have been already published [2)]. Each line corresponds to one case. Blue bars depict copy number gains, red bards copy number losses and yellow bars copy number neutral losses of heterozygosity. The minimal region of gain was defined as 11q23.2-q23.3 (chr11:114,081,947-118,434,149bp, hg19) and the minimal region of loss as (chr11:127,799,447-133,280,976bp, hg19) which overlapped with those described previously but reduced their sizes [2]. One case of the present series (4132817) harbored a focal homozygous loss in 11q24.2-q24.3, which overlaps with a homozygously deleted region in cases recently published[2,3].The most recurrently altered regions were besides the 11q-gain/loss, a partial trisomy 12q13.11-q24.32 (7/15 cases), gain in 7q34-qter and loss in 13q32.3-q34 each in 3/15 cases.

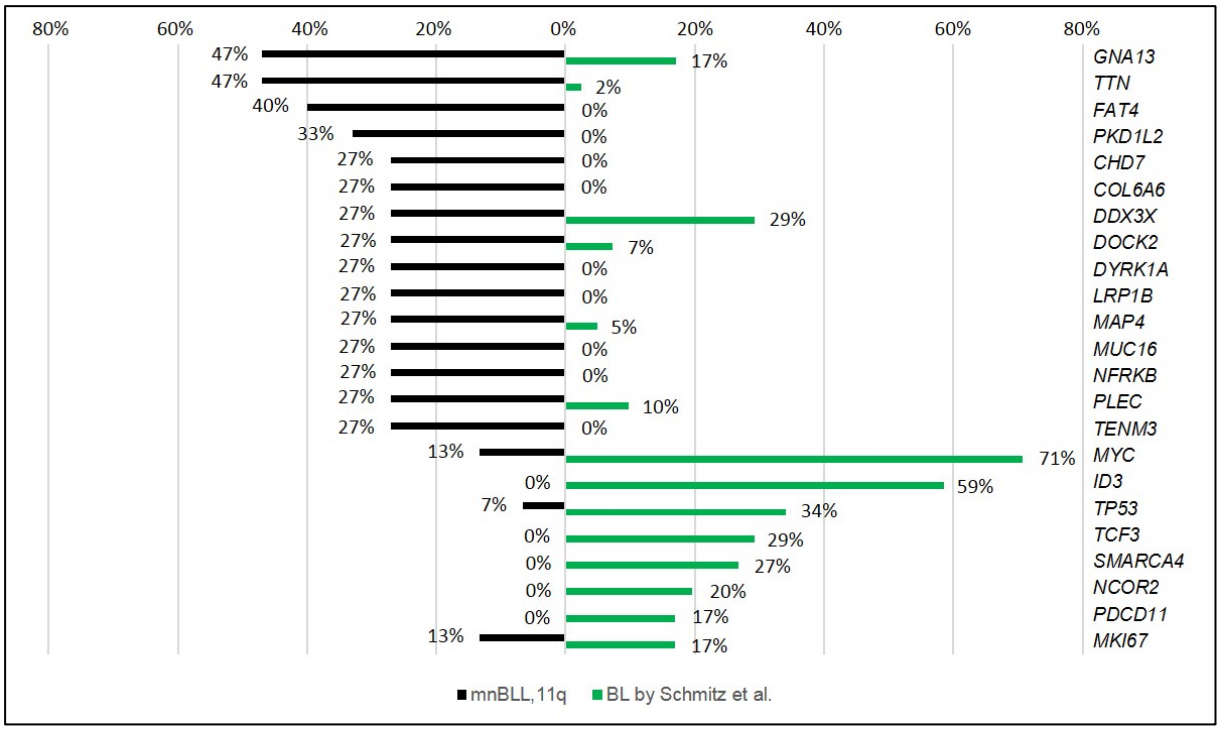

Supplemental Figure 2: Comparison of frequently mutated genes in mnBLL,11q, (black) and BL (green). Included are those genes which were reported by Schmitz et al.[26] to be recurrently mutated in at least 15% of BL cases (N=41 cases, 69,6% younger than 18 years at diagnosis) in the respective study as well as genes which were recurrently mutated in more than 15% of mnBLL,11q, cases. Using the published mutational landscape of BL by Schmitz et al.[26], we could show again that the highly recurrently mutated genes in BL were not or only rarely altered in mnBLL,11q. The exception to this are *DDX3X* and *GNA13*, which were recurrently mutated in both lymphoma entities (>15%).

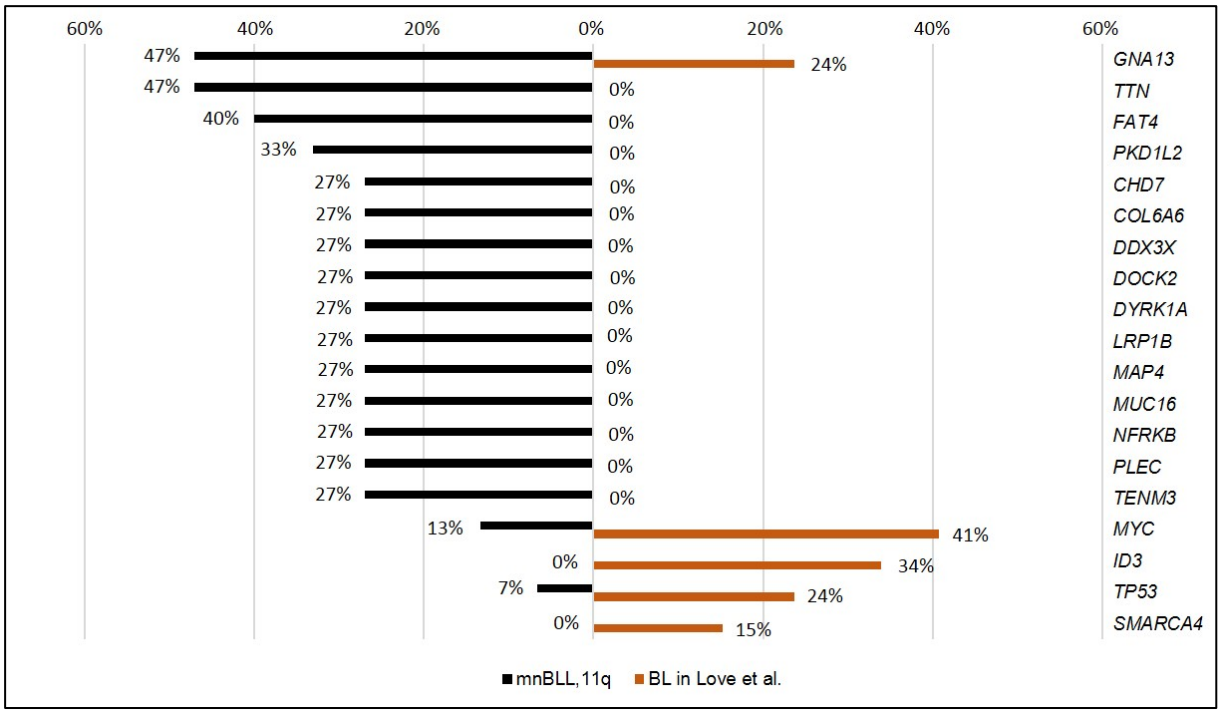

Supplemental Figure 3: Comparison of frequently mutated genes in mnBLL,11q, (black) and BL (orange). Included are those genes which were reported by Love et al.[27] to be recurrently mutated in at least 15% of BL cases (N=59 cases, median age at diagnosis, as available for 27 cases, was 19 (3-82) years) in the respective study as well as genes which were recurrently mutated in more than 15% of mnBLL,11q, cases. Using the published mutational landscape of BL by Love at al. [27], we could show again that the highly recurrently mutated genes in BL were not or only rarely altered in mnBLL,11q. The exception to this were the *GNA13* mutations occurring frequently in both lymphoma entities (>15%).

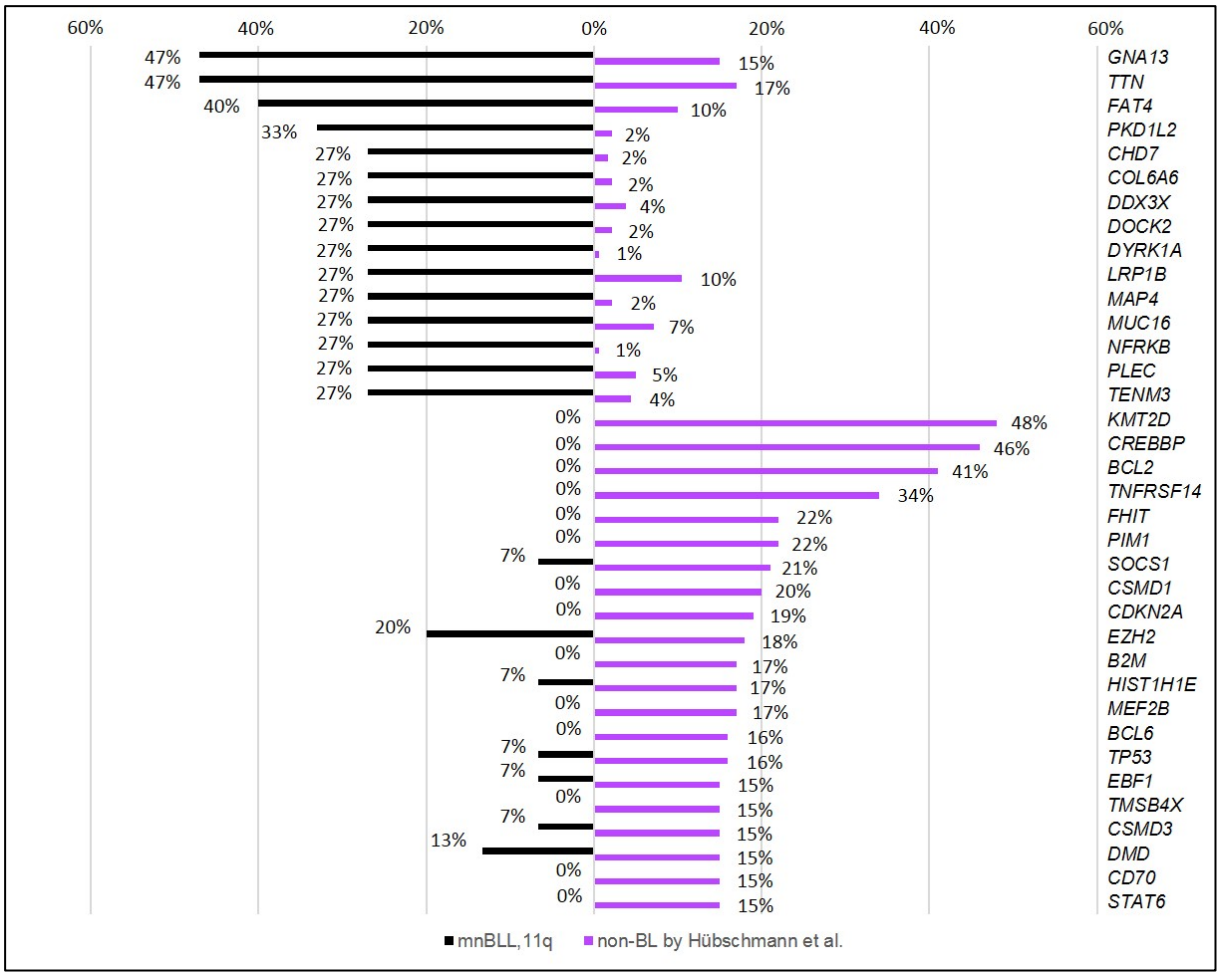

Supplemental Figure 4: Comparison of frequently mutated genes in 15 mnBLL,11q, cases (black) and 181 non-BL (median age at diagnosis 63 (range 33-89) years) including diffuse-large B cell lymphoma (DLBCL), follicular lymphoma (FL) and FL-DLBCL (violet). Included are those genes which were mutated in ≥15% of non-BL cases based on unpublished data from whole genome sequencing accessible at www.icgc.org (Hübschmann *et* al. submitted) as well as genes which were recurrently mutated in more than 15% of mnBLL,11q, cases. The mutational landscape of the mnBLL,11q cases was overall different than that from non-BL samples. Nevertheless, few genes were recurrently mutated in both lymphoma groups including *EZH2, GNA13* and *TTN* (≥15%).

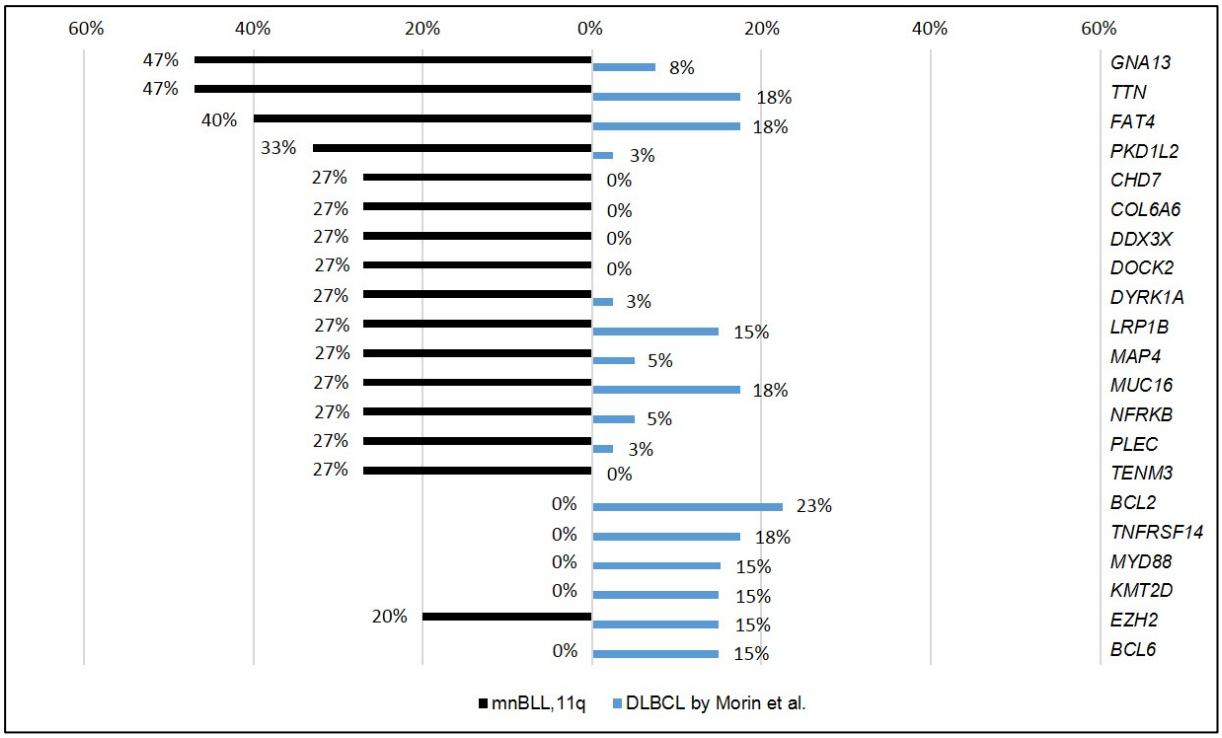

Supplemental Figure 5: Comparison of frequently mutated genes in mnBLL,11q, (black) and diffuse-large B cell lymphoma (DLBCL) (blue). Included are those genes which were mutated in ≥15% of DLBCL as reported by Morin et al.[28] (age at diagnosis unknown) as well as genes which were recurrently mutated in more than 15% of mnBLL,11q, cases. Few genes were recurrently mutated in both lymphoma entities including *EZH2*, *TTN, FAT4,* as well as *MUC16* (>15%).

Remarkably, exome analyses in recently published large series of DLBCL[29–32] have only rarely reported protein-changing *NFRKB* mutations in DLBCL (total 22/1031 DLBLC (2%) based on [30–32]). The gene was moreover not detected as driver gene in DLBCL by Reddy *et* al.[29]. Mining the publically available data by Reddy et al.[29] identified 21 pediatric/young adult DLBCL cases (<25 years at diagnosis) for which the driver gene mutations per case were provided. Of the 150 driver genes, only two overlap with the genes we identified as frequently mutated in mnBLL,11q, namely *GNA13* and *DDX3X*. These were mutated in only 1/21 and 0/21 of the pediatric/young adulthood DLBLC cases, respectively. Hence, we can indirectly (absence of *NFRKB* as driver gene) and directly (frequency of driver gene mutations) conclude from this data that the mutational spectrum of mnBLL,11q, is quite different from that of pediatric/young adult DLBCL.

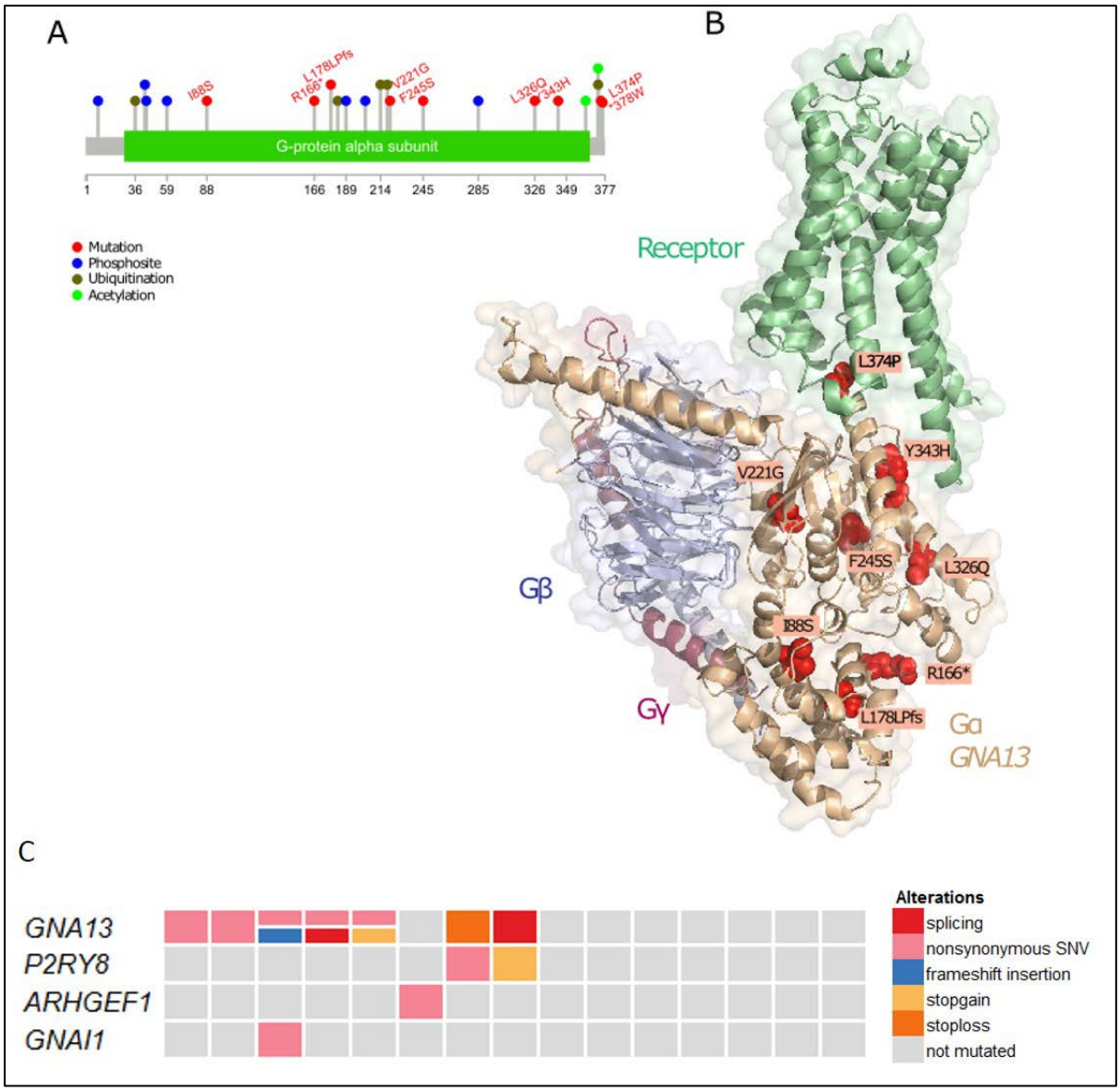

Supplemental Figure 6: (A) Localization of the *GNA13* mutations (red lollipos) annotated on protein primary sequence (based on ENST00000439174.2) with additional information regarding post-translocation modifications (PTMs) and domain composition. The majority of mutations were nonsynonymous, which are located within the catalytic Ras and α-helical domains of the G-protein alpha subunit. The stopgain mutation leads to a loss of the C-terminal part of the protein. The stopgain mutation leads to a loss of the C-terminal part of the protein.
(B) Mutated residues (red spheres) shown on a model of heterotrimeric G13 (Gα in wheat, Gβ in blue and Gγ in raspberry) bound to a G-protein coupled receptor (green). The prototypical structure of ADRB2 receptor complexed to Gs heterotrimer (PDB ID: 3SN6) has been used as a template to model the quaternary complex (see Methods section “Mutation modeling”).
(C) Depicted are the protein changing mutations within the $G_{12/13}$ and $G_{i}\alpha$ signaling pathway[33]. The columns encode samples and the rows different genes. Different mutation types are color-coded in the oncoprint, where different types of mutation can coexist in one sample. 53% (8/15) of mnBLL,11q, cases harbored a mutation within this signaling pathway.

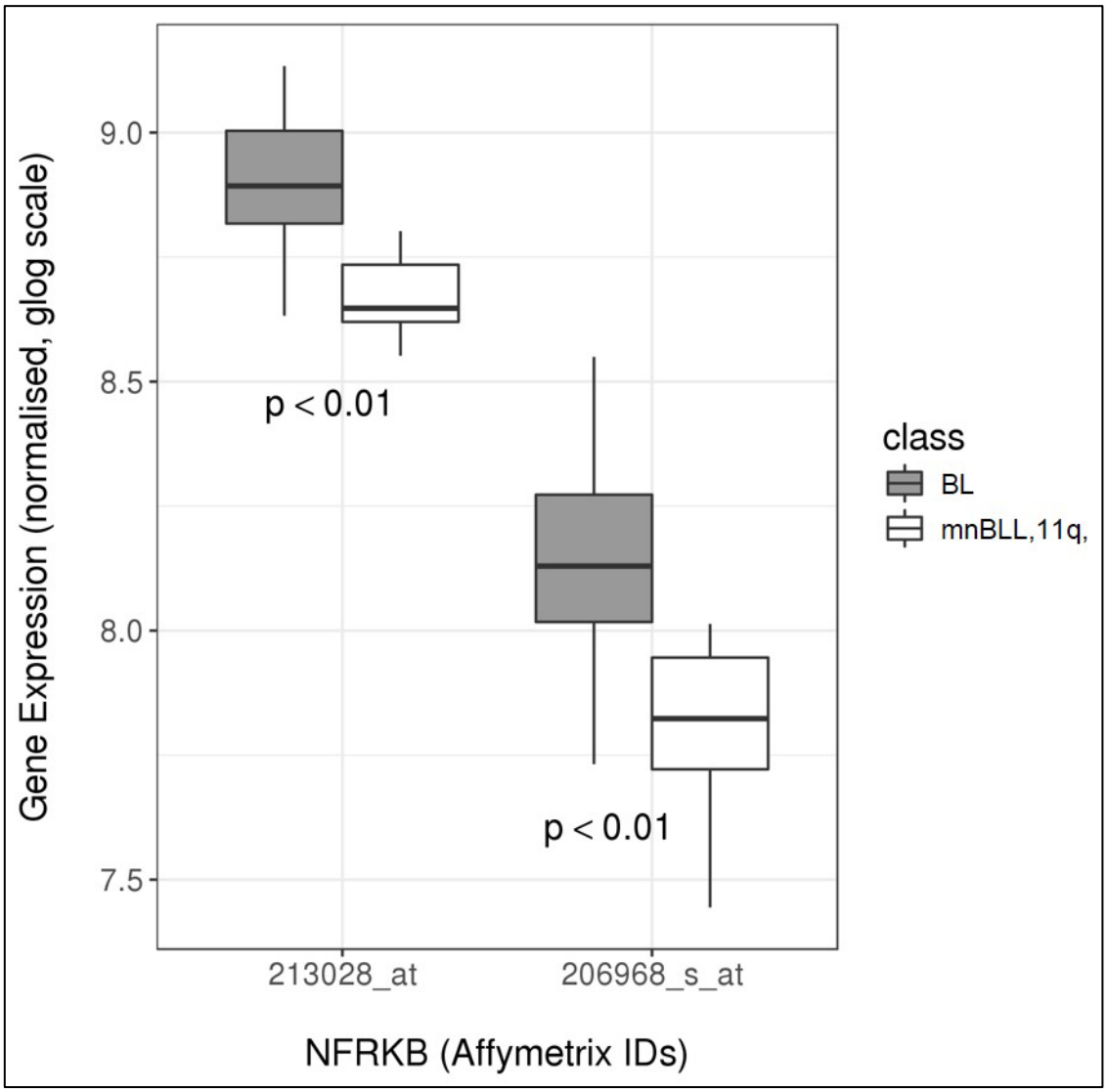

Supplemental Figure 7: NFRKB expression levels in mnBLL,11q, cases and Burkitt lymphoma (BL) based on Affymetrix U133A expression arrays as published by [2]. The boxplots show that NFRKB is significantly lower expressed in the mnBLL,11q, cases compared to BL (adj. p<0.01).

SUPPLEMENTAL REFERENCES

1. Pienkowska-Grela B, Rymkiewicz G, Grygalewicz B, et al. Partial trisomy 11, dup(11)(q23q13), as a defect characterizing lymphomas with Burkitt pathomorphology without MYC gene rearrangement. *Med. Oncol.* 2011;28(4):1589–1595.
2. Salaverria I, Martin-Guerrero I, Wagener R, et al. A recurrent 11q aberration pattern characterizes a subset of MYC-negative high-grade B-cell lymphomas resembling Burkitt lymphoma. *Blood*. 2014;123(8):1187–1198.
3. Rymkiewicz G, Grygalewicz B, Chechlinska M, et al. A comprehensive flow-cytometry-based immunophenotypic characterization of Burkitt-like lymphoma with 11q aberration. *Mod. Pathol.* 2018;31(5):732–743.
4. Bonetti P, Testoni M, Scandurra M, et al. Deregulation of ETS1 and FLI1 contributes to the pathogenesis of diffuse large B-cell lymphoma. *Blood*. 2013;122(13):2233–2241.
5. Scholtysik R, Kreuz M, Hummel M, et al. Characterization of genomic imbalances in diffuse large B-cell lymphoma by detailed SNP-chip analysis. *Int. J. Cancer*. 2015;136(5):1033–1042.
6. Ventura RA, Martin-Subero JI, Jones M, et al. FISH analysis for the detection of lymphoma-associated chromosomal abnormalities in routine paraffin-embedded tissue. *J Mol Diagn*. 2006;8(2):141–151.
7. Martín-Subero JI, Harder L, Gesk S, et al. Interphase FISH assays for the detection of translocations with breakpoints in immunoglobulin light chain loci. *Int. J. Cancer*. 2002;98(3):470–474.
8. Hummel M, Bentink S, Berger H, et al. A biologic definition of Burkitt's lymphoma from transcriptional and genomic profiling. *N. Engl. J. Med.* 2006;354(23):2419–2430.
9. Wagener R, López C, Kleinheinz K, et al. IG-MYC+ neoplasms with precursor B-cell phenotype are molecularly distinct from Burkitt lymphomas. *Blood*. 2018;132(21):2280–2285.
10. Li H, Handsaker B, Wysoker A, et al. The Sequence Alignment/Map format and SAMtools. *Bioinformatics*. 2009;25(16):2078–2079.
11. Sherry ST, Ward MH, Kholodov M, et al. dbSNP: the NCBI database of genetic variation. *Nucleic Acids Res.* 2001;29(1):308–311.
12. Jabs J, Zickgraf FM, Park J, et al. Screening drug effects in patient-derived cancer cells links organoid responses to genome alterations. *Mol. Syst. Biol.* 2017;13(11):955.
13. Lek M, Karczewski KJ, Minikel EV, et al. Analysis of protein-coding genetic variation in 60,706 humans. *Nature*. 2016;536(7616):285–291.
14. Nik-Zainal S, Alexandrov LB, Wedge DC, et al. Mutational processes molding the genomes of 21 breast cancers. *Cell*. 2012;149(5):979–993.
15. Lawrence MS, Stojanov P, Polak P, et al. Mutational heterogeneity in cancer and the search for new cancer-associated genes. *Nature*. 2013;499(7457):214–218.
16. Reva B, Antipin Y, Sander C. Predicting the functional impact of protein mutations: application to cancer genomics. *Nucleic Acids Res.* 2011;39(17):e118.
17. McLaren W, Gil L, Hunt SE, et al. The Ensembl Variant Effect Predictor. *Genome Biol.* 2016;17(1):122.
18. Betts MJ, Lu Q, Jiang Y, et al. Mechismo: predicting the mechanistic impact of mutations and modifications on molecular interactions. *Nucleic Acids Res.* 2015;43(2):e10.
19. Jay JJ, Brouwer C. Lollipops in the Clinic: Information Dense Mutation Plots for Precision Medicine. *PLoS ONE*. 2016;11(8):e0160519.
20. Hornbeck PV, Zhang B, Murray B, et al. PhosphoSitePlus, 2014: mutations, PTMs and recalibrations. *Nucleic Acids Res.* 2015;43(Database issue):D512-520.
21. Sali A, Blundell TL. Comparative protein modelling by satisfaction of spatial restraints. *J. Mol. Biol.* 1993;234(3):779–815.
22. Yao T, Song L, Jin J, et al. Distinct modes of regulation of the Uch37 deubiquitinating enzyme in the proteasome and in the Ino80 chromatin-remodeling complex. *Mol. Cell*. 2008;31(6):909–917.
23. Zediak VP, Berger SL. Hit and run: transient deubiquitylase activity in a chromatin-remodeling complex. *Mol. Cell*. 2008;31(6):773–774.
24. Sahtoe DD, van Dijk WJ, El Oualid F, et al. Mechanism of UCH-L5 activation and inhibition by DEUBAD domains in RPN13 and INO80G. *Mol. Cell*. 2015;57(5):887–900.
25. Davis CA, Hitz BC, Sloan CA, et al. The Encyclopedia of DNA elements (ENCODE): data portal update. *Nucleic Acids Res.* 2018;46(D1):D794–D801.
26. Schmitz R, Young RM, Ceribelli M, et al. Burkitt lymphoma pathogenesis and therapeutic targets from structural and functional genomics. *Nature*. 2012;490(7418):116–120.
27. Love C, Sun Z, Jima D, et al. The genetic landscape of mutations in Burkitt lymphoma. *Nat. Genet.* 2012;44(12):1321–1325.

28. Morin RD, Mungall K, Pleasance E, et al. Mutational and structural analysis of diffuse large B-cell lymphoma using whole-genome sequencing. *Blood*. 2013;122(7):1256–1265.
29. Reddy A, Zhang J, Davis NS, et al. Genetic and Functional Drivers of Diffuse Large B Cell Lymphoma. *Cell*. 2017;171(2):481-494.e15.
30. Arthur SE, Jiang A, Grande BM, et al. Genome-wide discovery of somatic regulatory variants in diffuse large B-cell lymphoma. *Nat Commun*. 2018;9(1):4001.
31. Chapuy B, Stewart C, Dunford AJ, et al. Molecular subtypes of diffuse large B cell lymphoma are associated with distinct pathogenic mechanisms and outcomes. *Nat. Med.* 2018;24(5):679–690.
32. Schmitz R, Wright GW, Huang DW, et al. Genetics and Pathogenesis of Diffuse Large B-Cell Lymphoma. *N. Engl. J. Med.* 2018;378(15):1396–1407.
33. Muppidi JR, Schmitz R, Green JA, et al. Loss of signalling via Gα13 in germinal centre B-cell-derived lymphoma. *Nature*. 2014;516(7530):254–258.

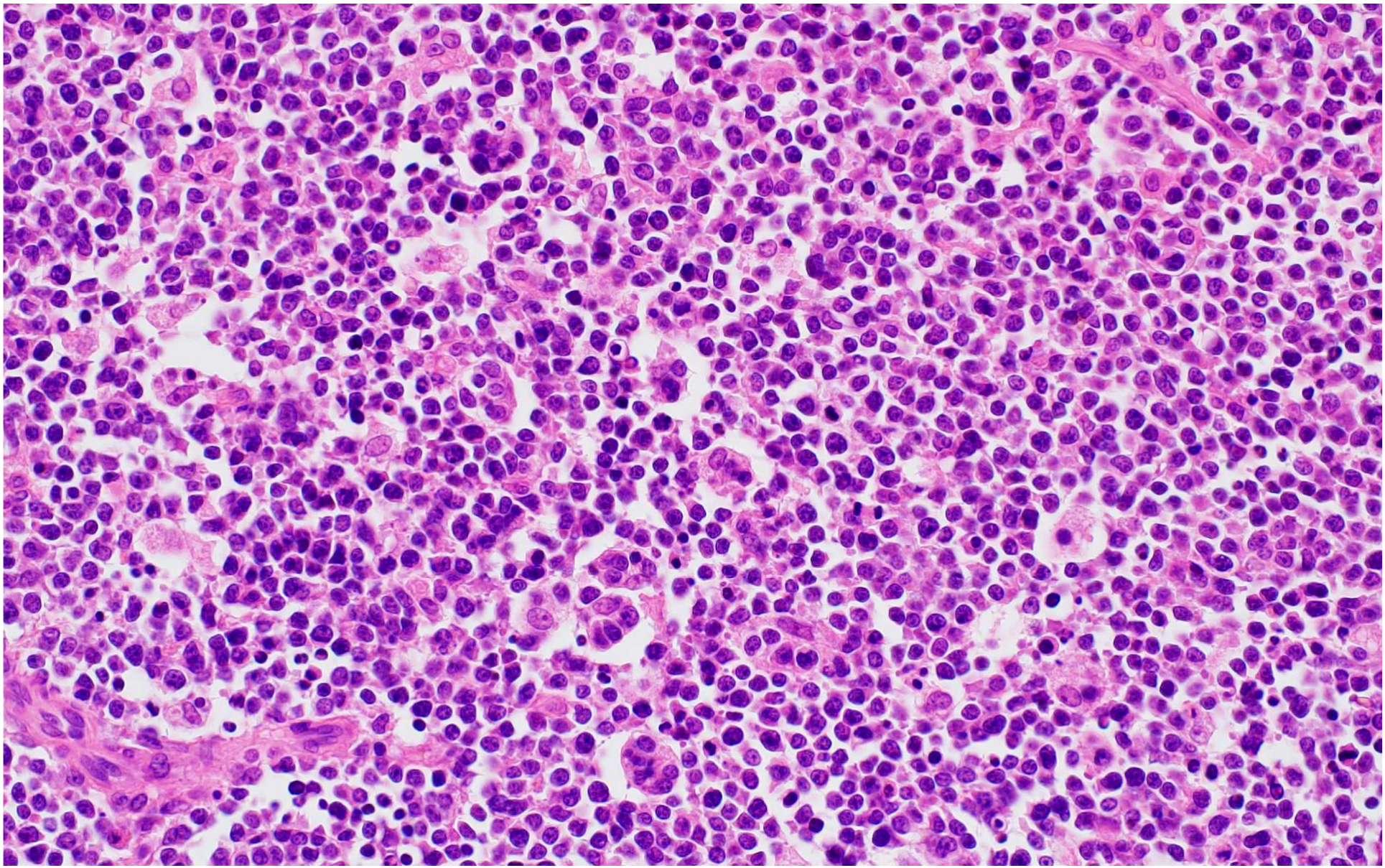

4130889, 400x

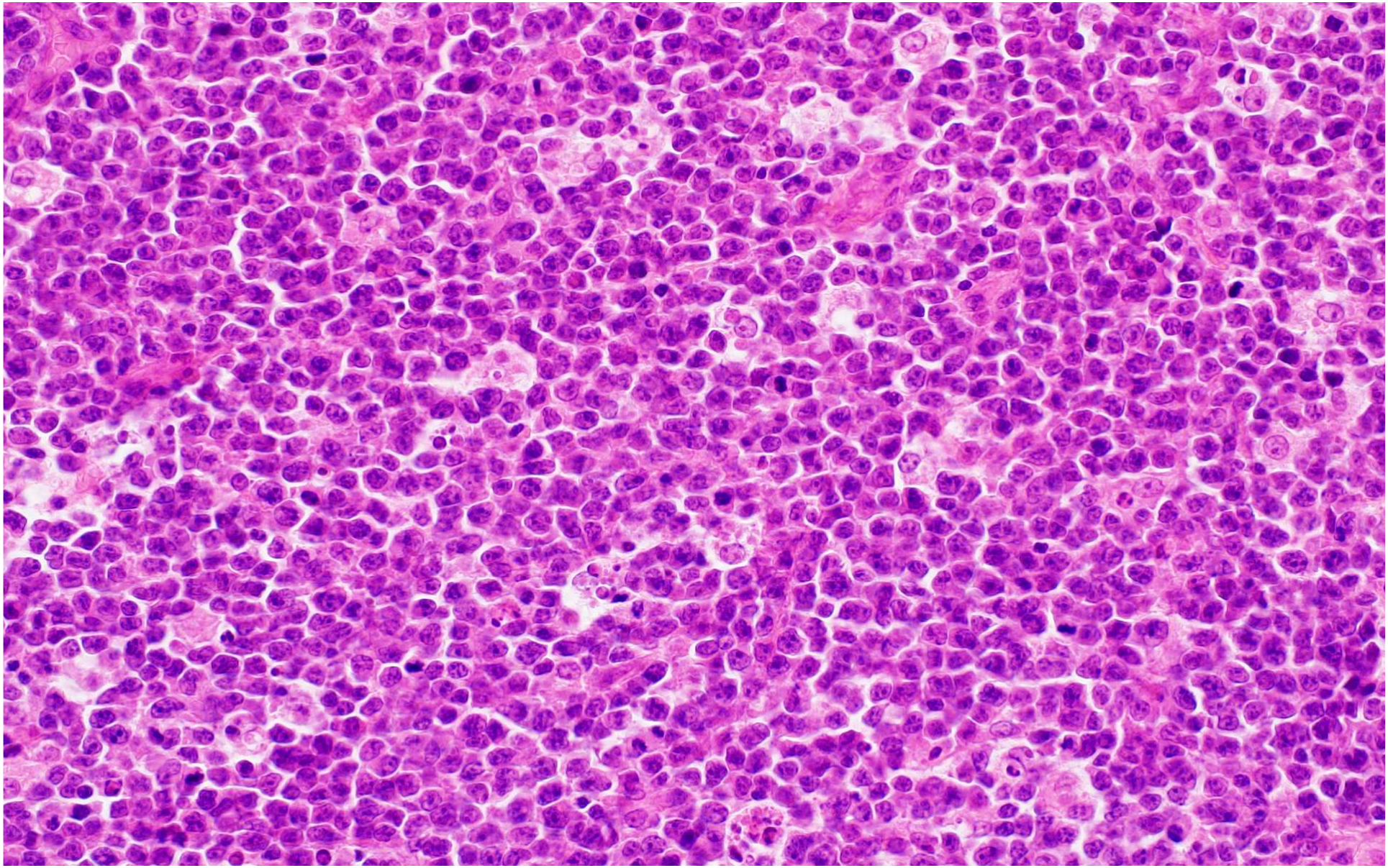

4132029, 400x

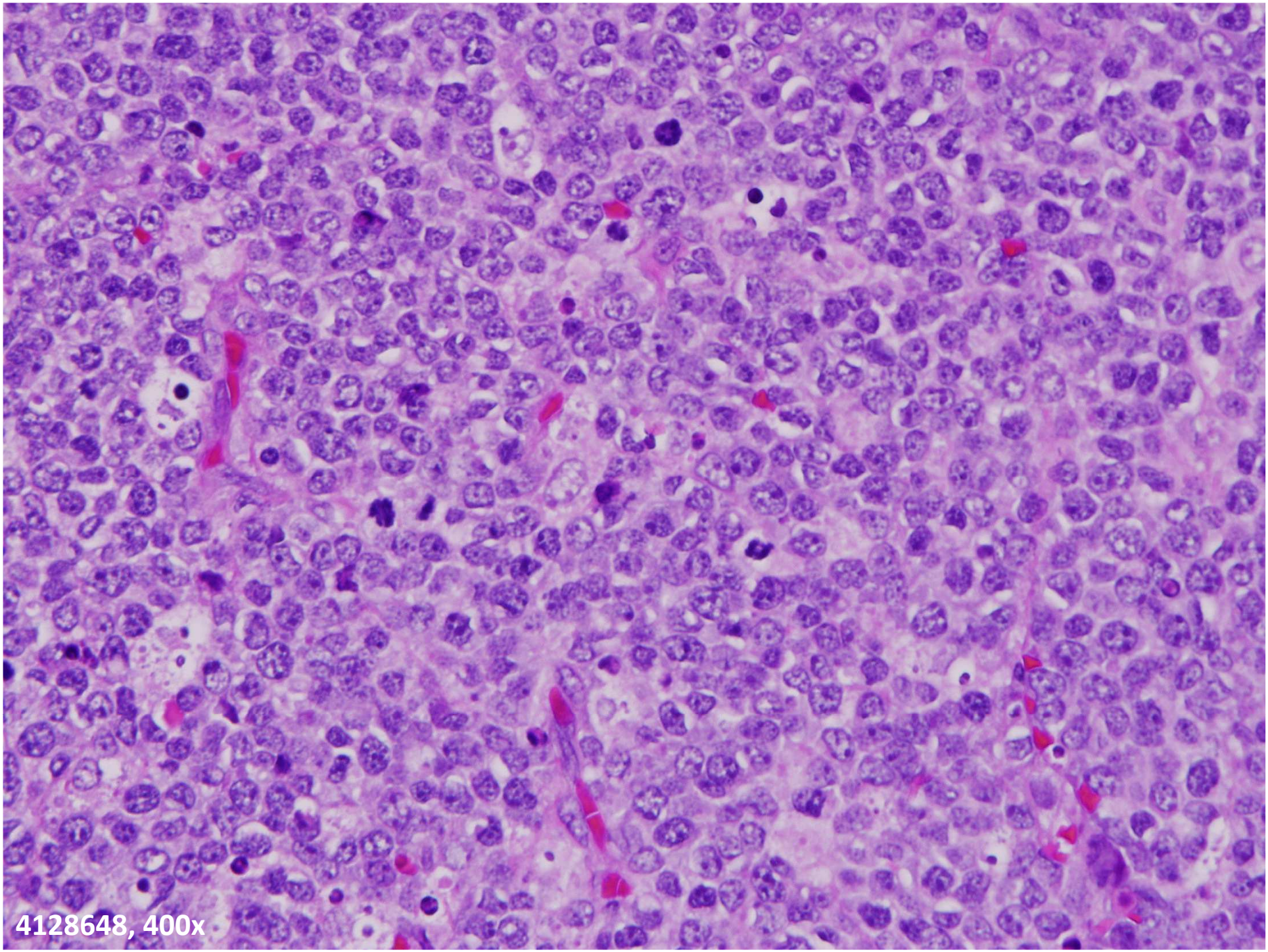
4128648, 400x

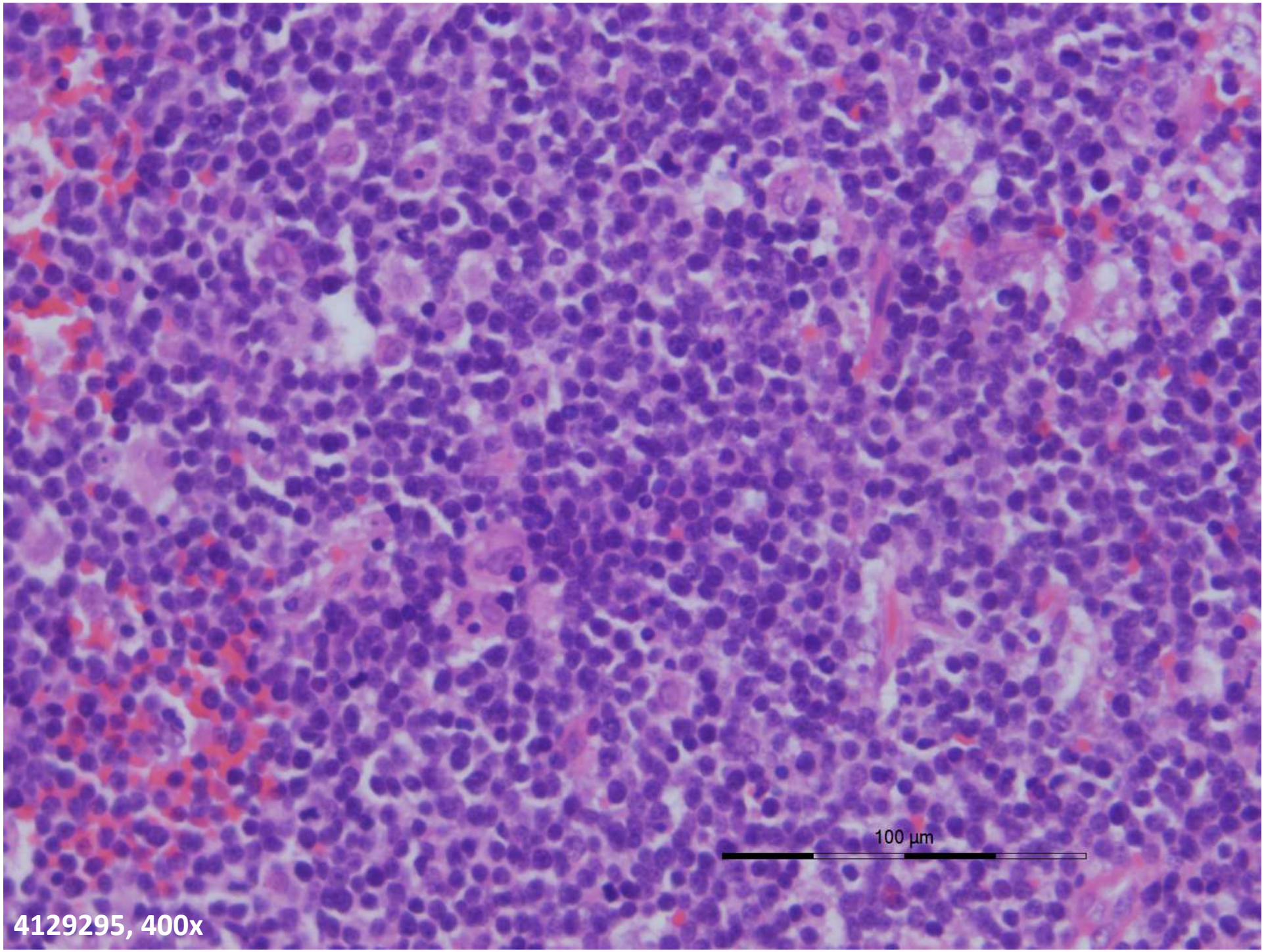
100 µm
4129295, 400x

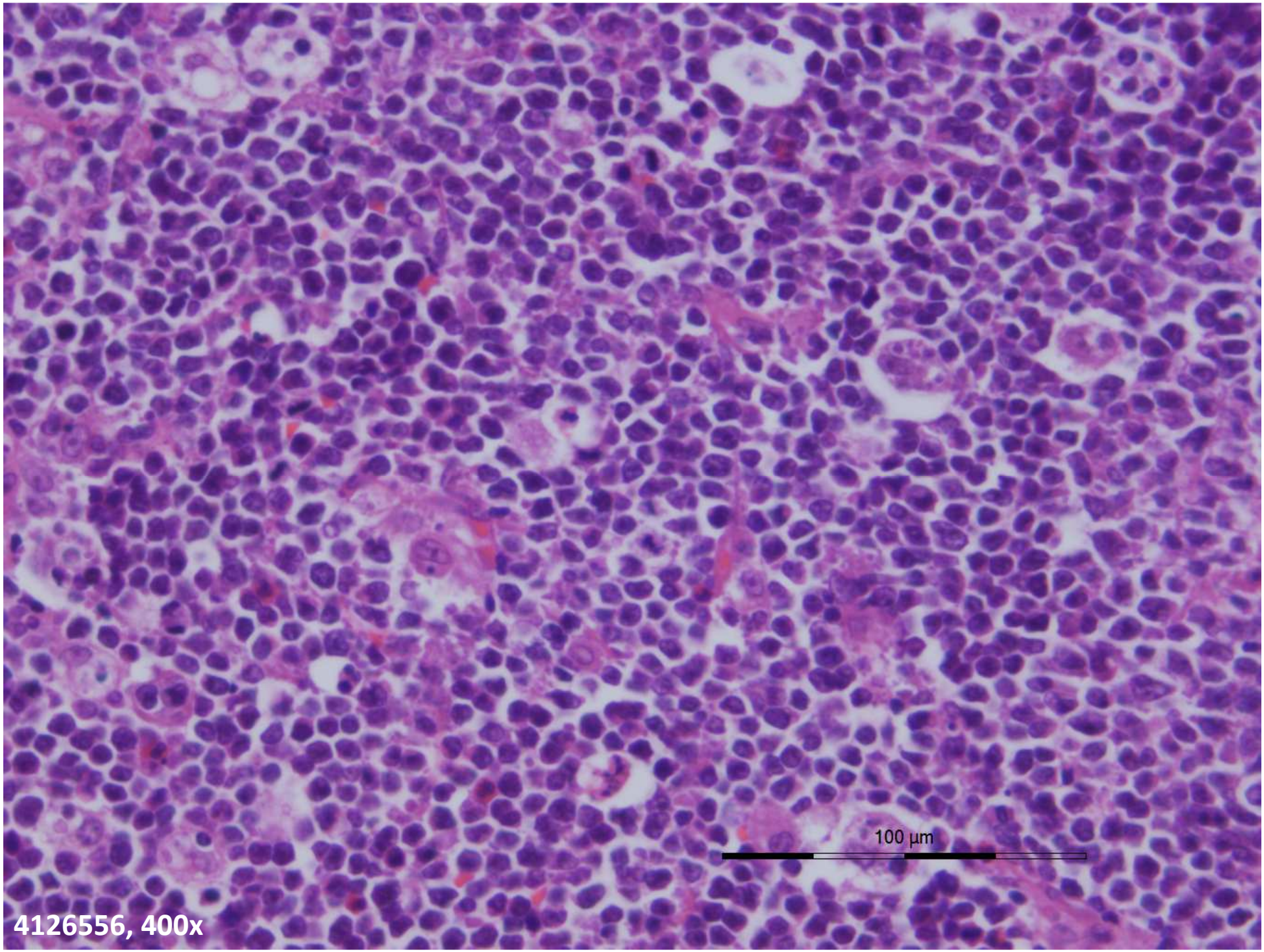
100 µm
4126556, 400x

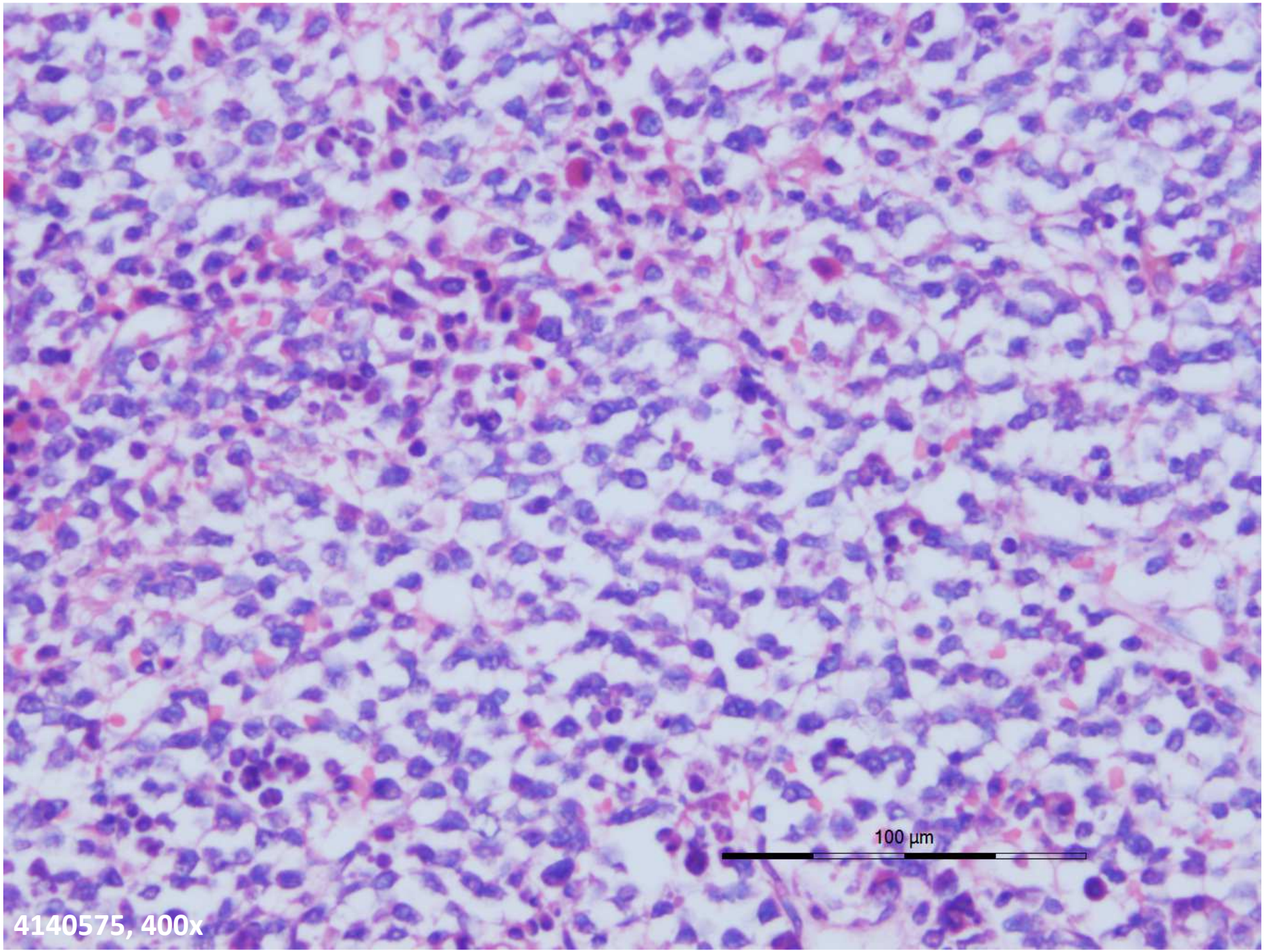
100 µm
4140575, 400x

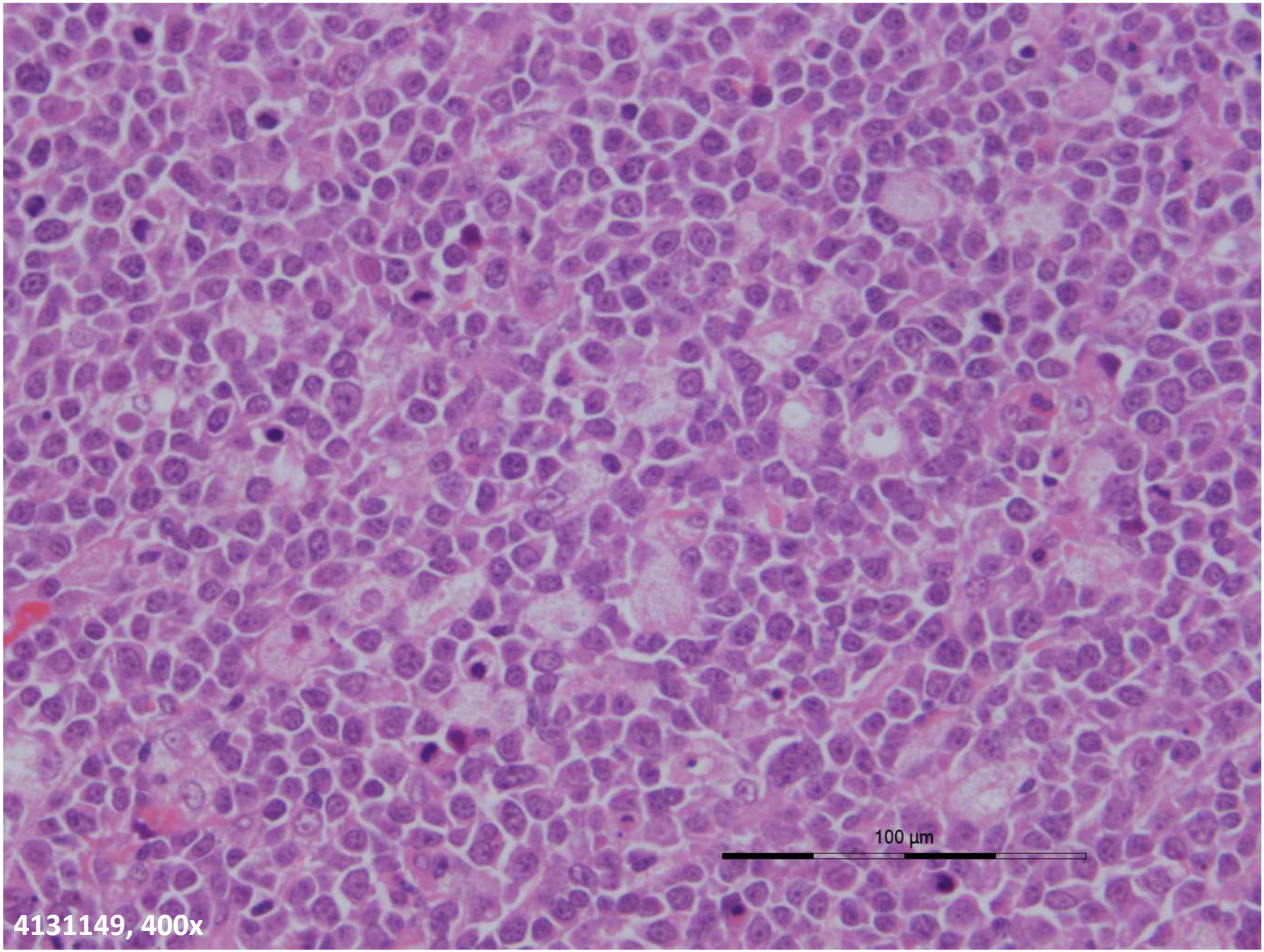
100 µm
4131149, 400x

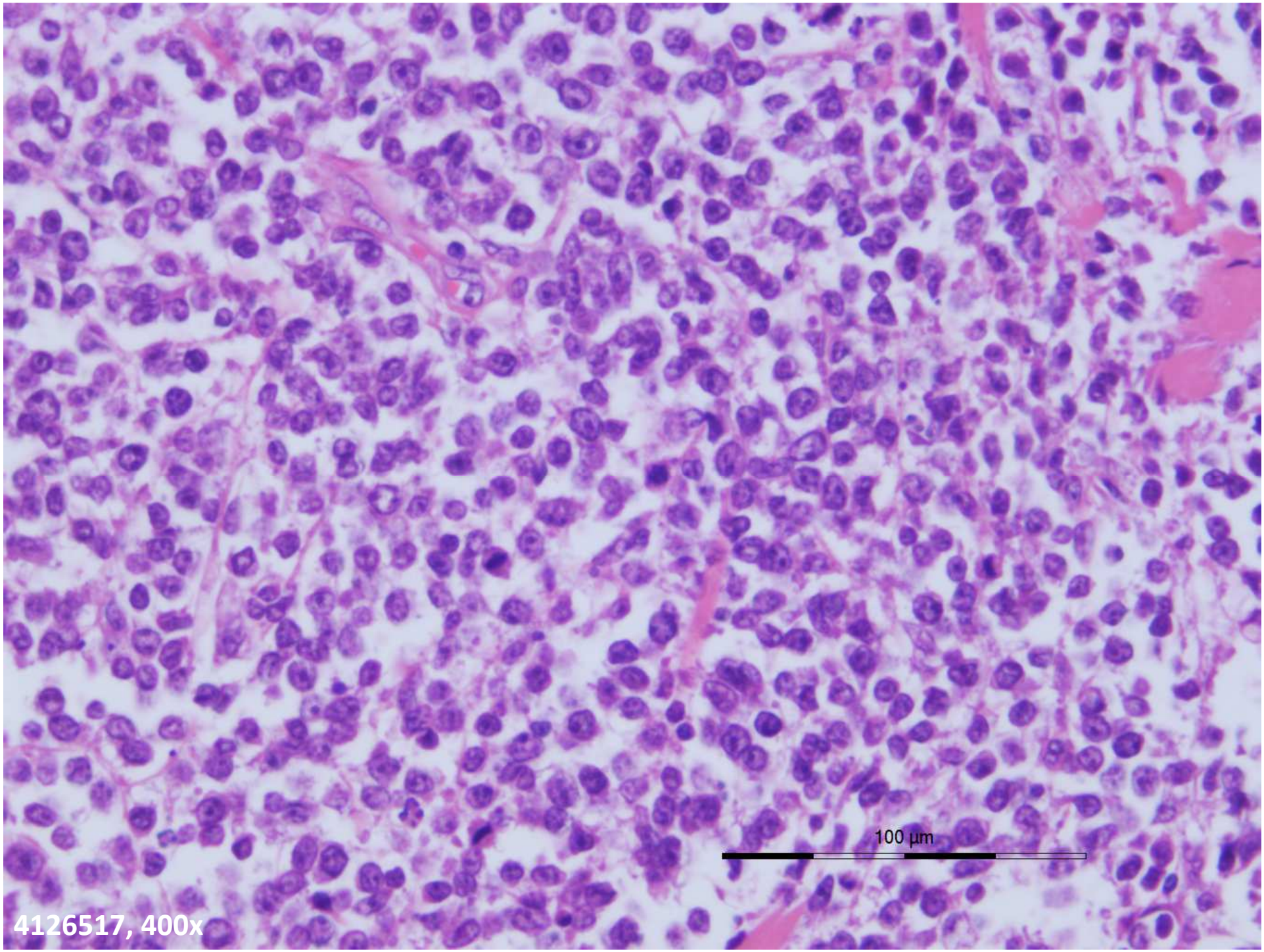
100 µm
4126517, 400x

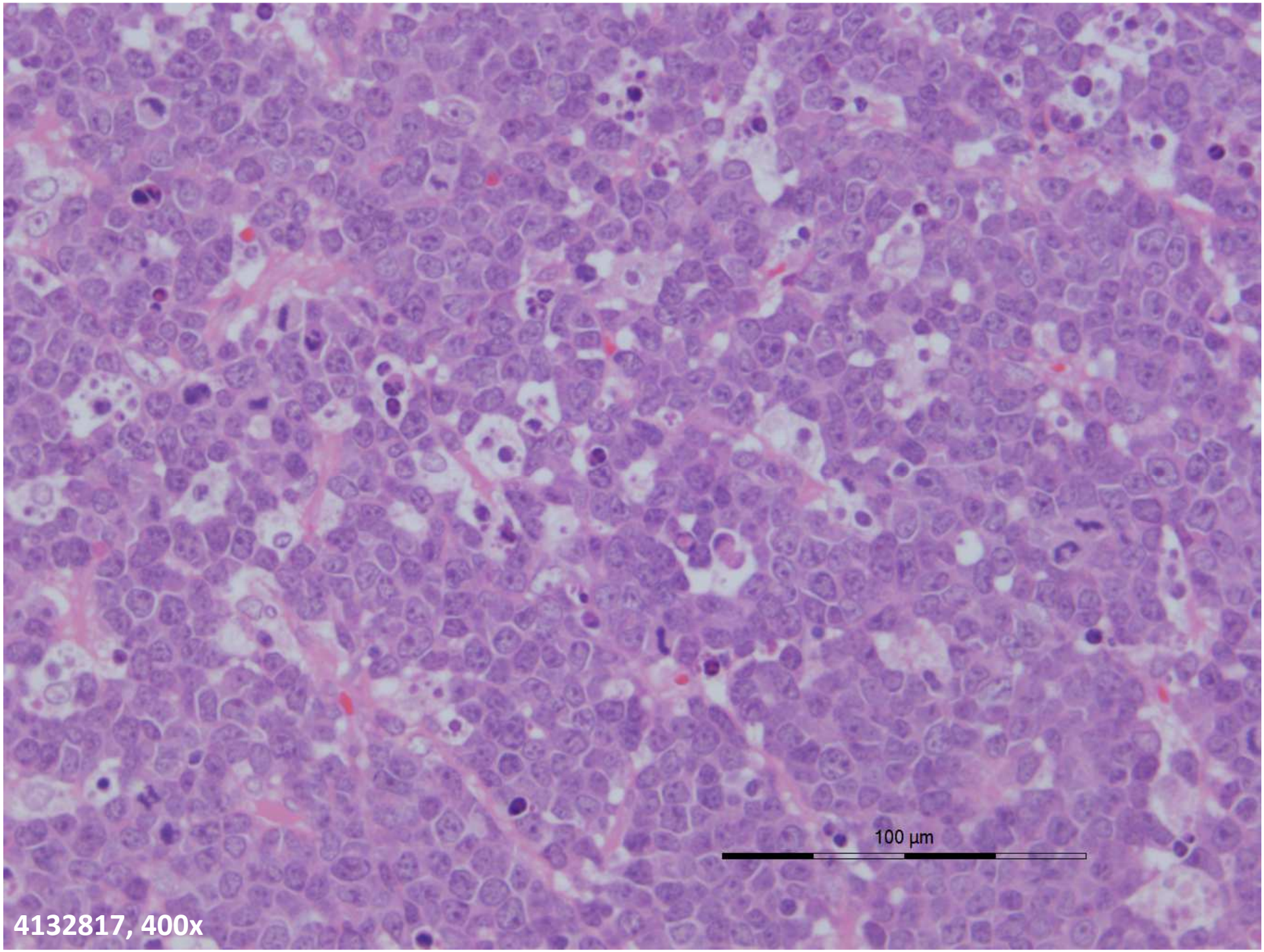
100 µm
4132817, 400x

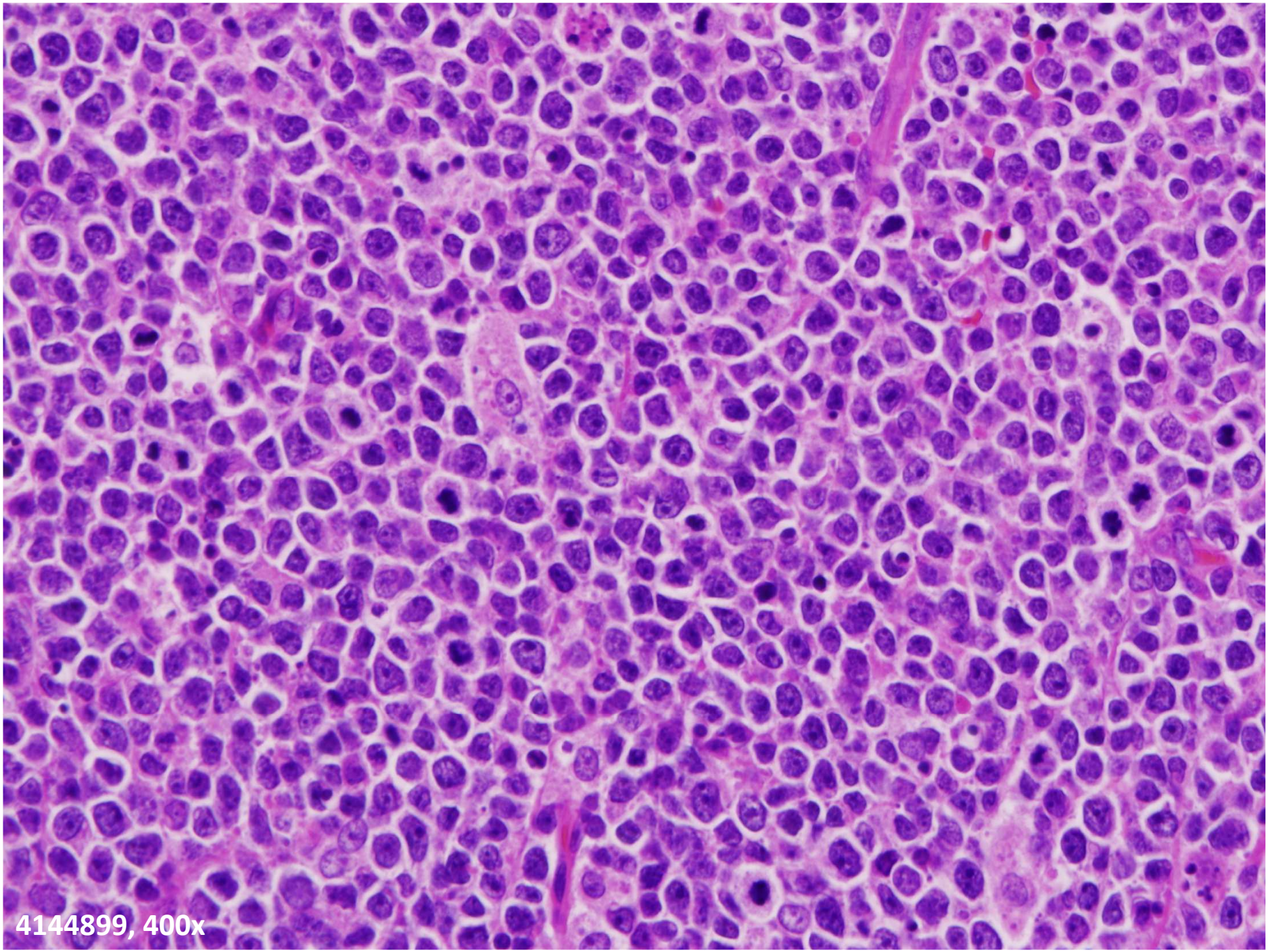
4144899, 400x

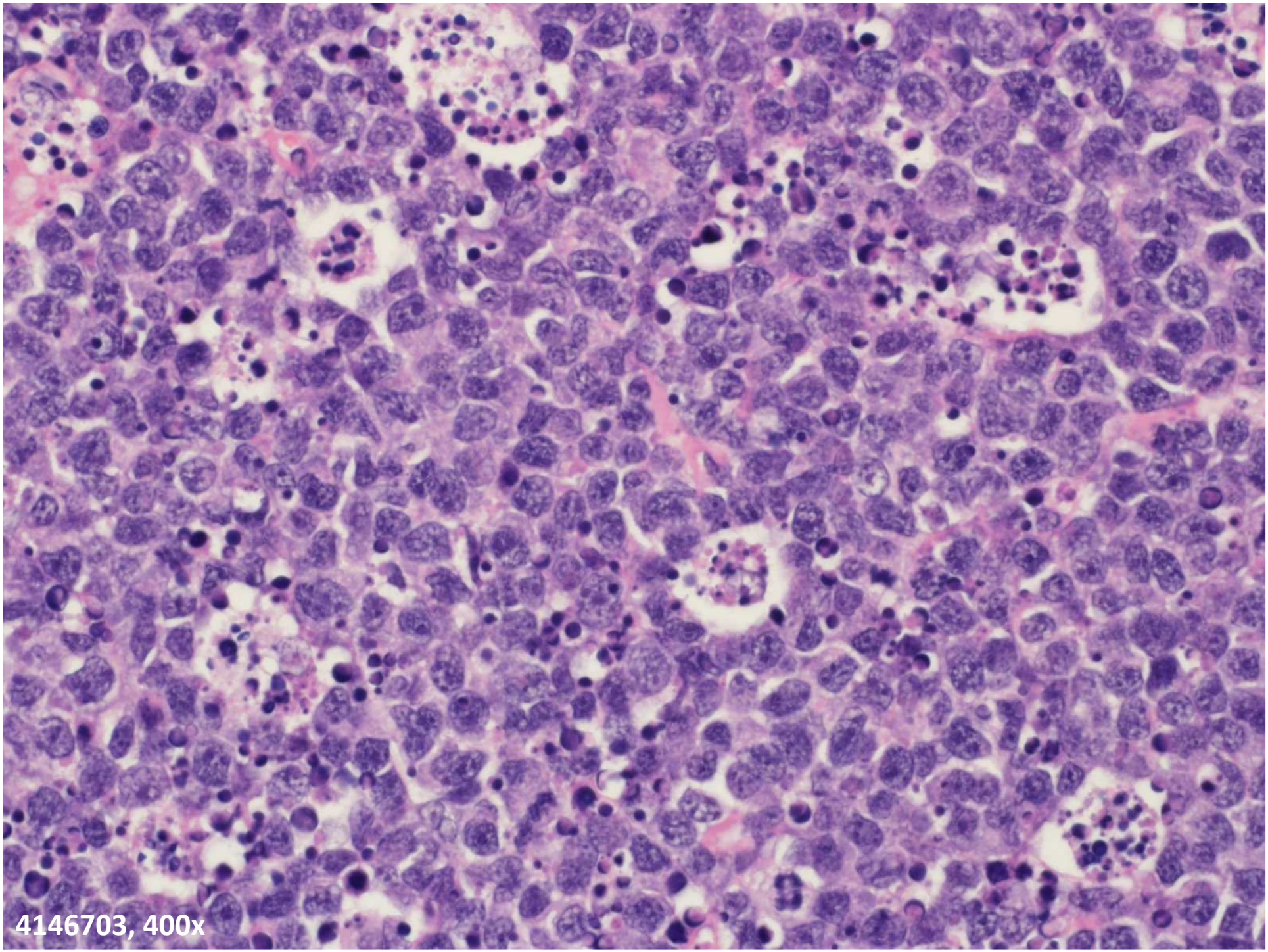
4146703, 400x

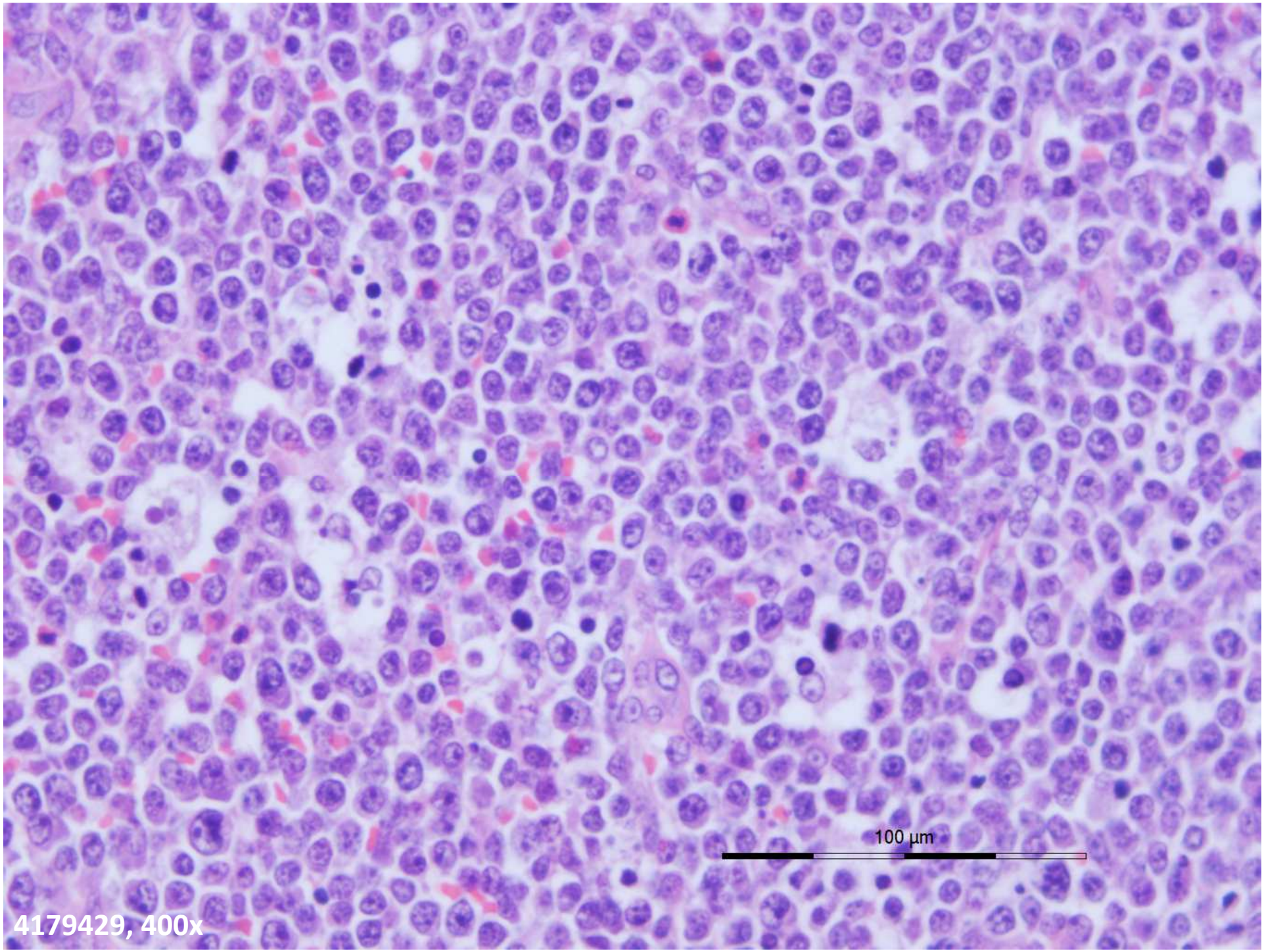
100 µm
4179429, 400x

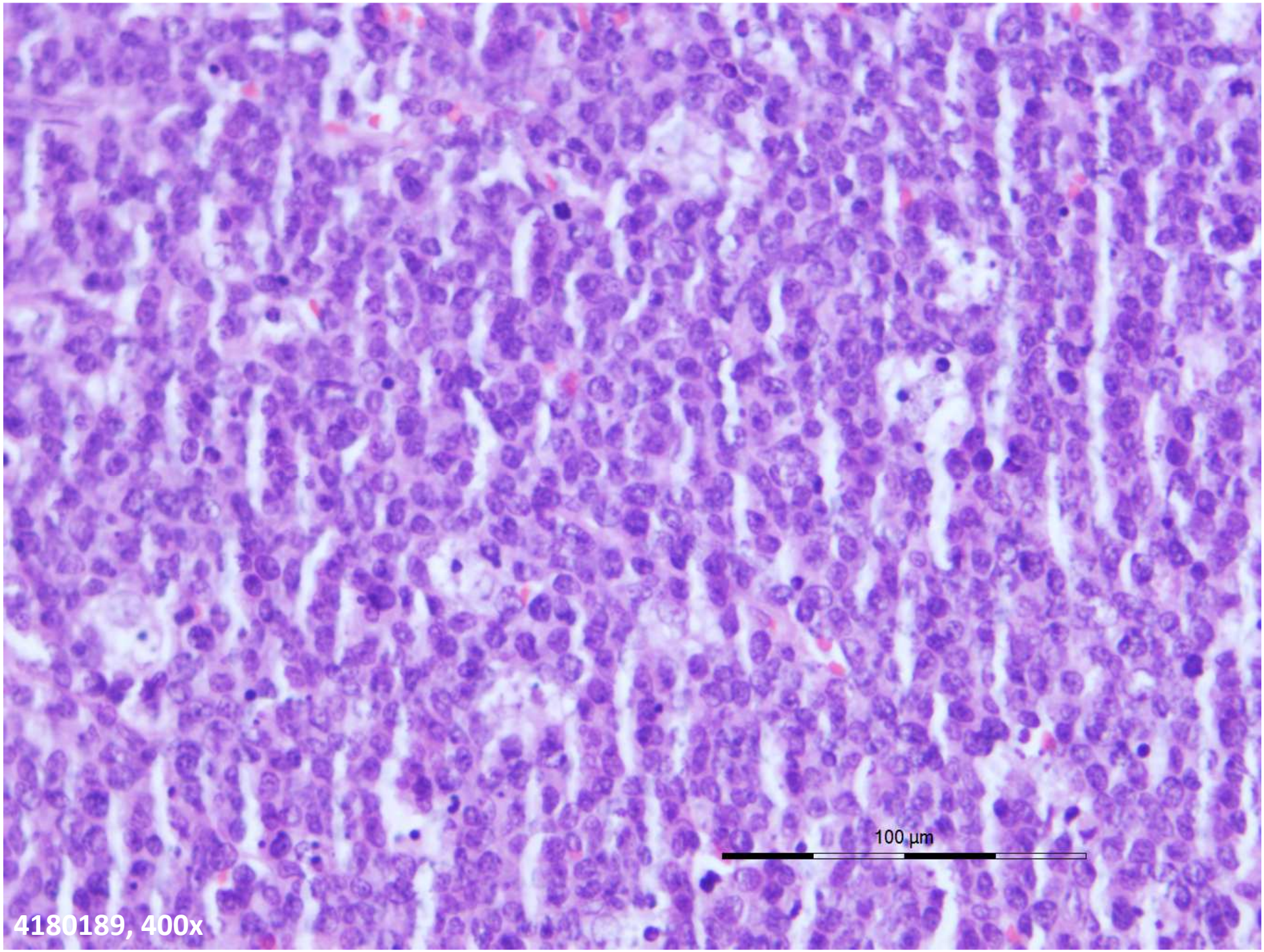
100 µm
4180189, 400x

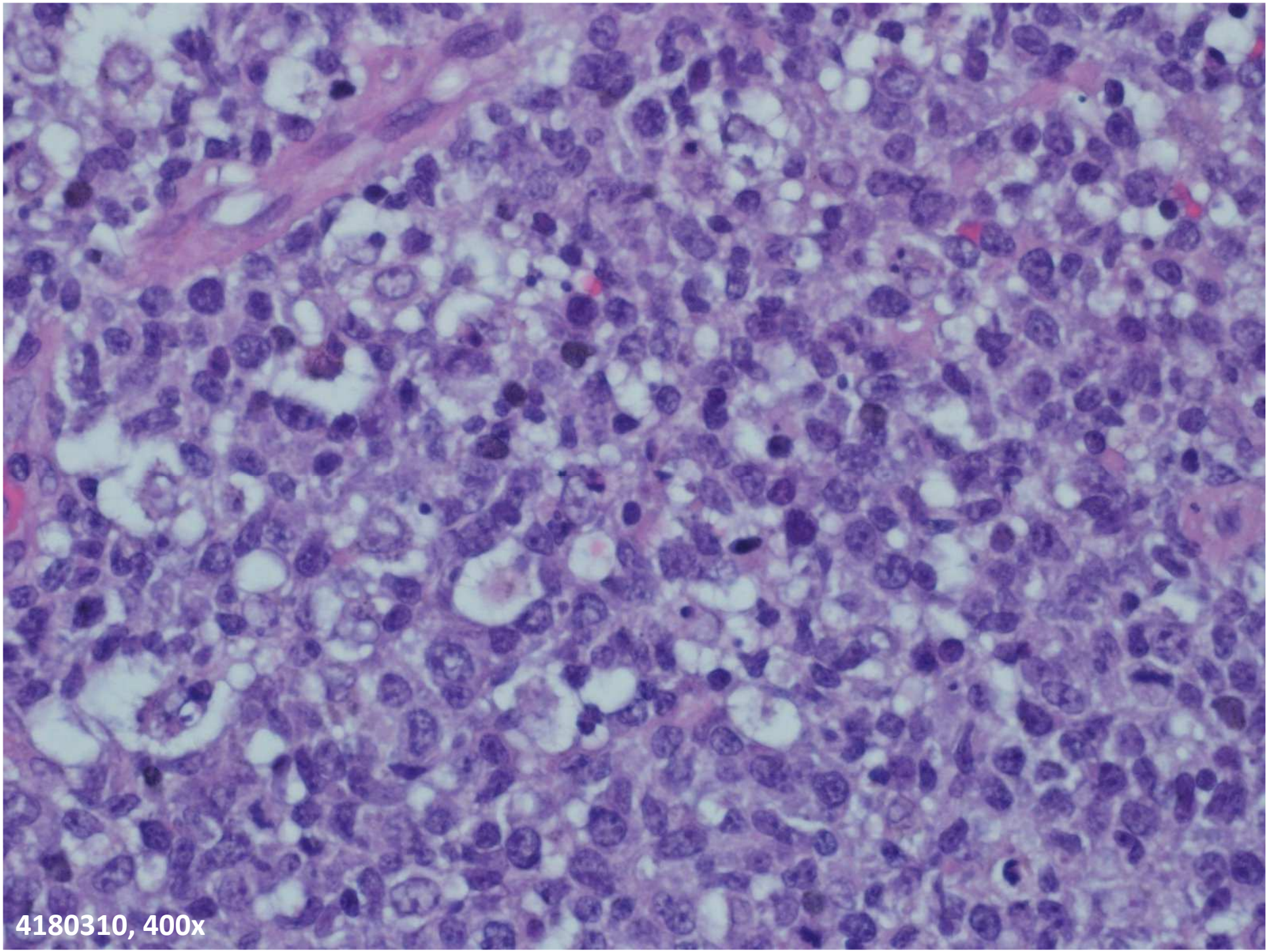
4180310, 400x

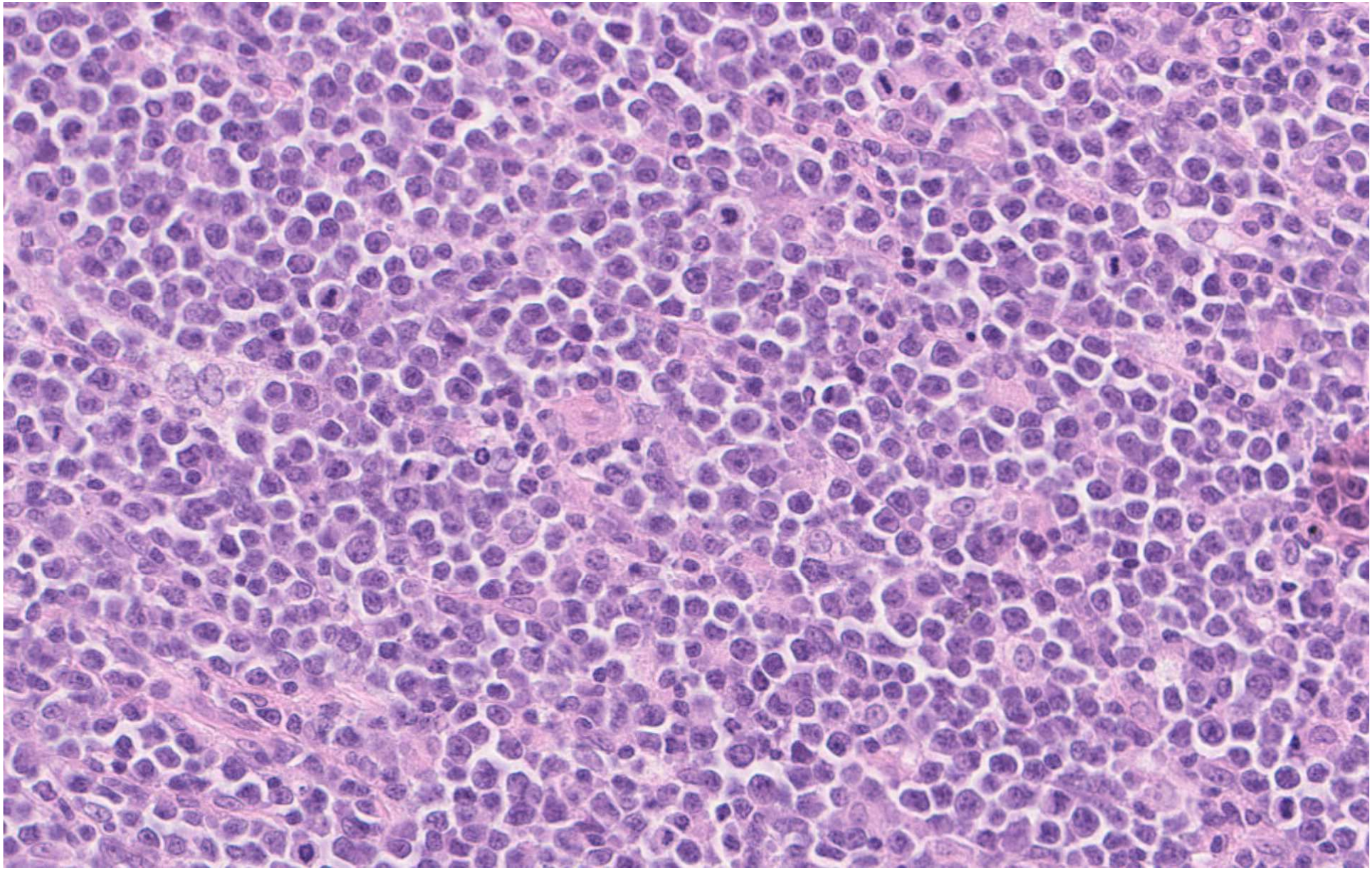

4181370, 400x